NTNU
Norwegian University of
Science and Technology

Pump as Turbine

Symmetry Prediction Method for Pump as
Turbine Characteristics

Øyvind Albert

Master of Energy and Environmental Engineering
Submission date: June 2018
Supervisor: Torbjørn Kristian Nielsen, EPT
Co-supervisor: Mdee Ombeni, UDSM

Norwegian University of Science and Technology
Department of Energy and Process Engineering

NTNU

Norwegian University
of Science and Technology

Department of Energy
and Process Engineering

EPT-M-2018-06

MASTER THESIS

for

Student Øyvind Albert

Spring 2018

Pump as Turbine (PAT)

Pumpe som turbin (PAT)

Background and objective

For small hydro power plants, both in Norway and in developing countries, the issue is to reduce the turbine price as far as possible. Efficiency has not necessary the highest priority. A centrifugal pump run in reverse is good choice. It has relative good efficiency, it is a robust construction and much cheaper than a turbine. The main reason for the low price is that pumps are mas-produced and there is no wicket gate. The problem is to pick the right pump for given Head and Flow.

We have a PhD student at University of Dar es Salam (UDSM) working on PAT supported by a Norad program (EnPe), and we would like the Norwegian student to be collaborating with him and, if possible, perform tests at Dar es Salam University.

The objective is to veryfy the method described in the Project Work of how to predict the performance of a pump when running as turbine.

The project shall be done in cooperation with stud Sondre Skjoldli

The following tasks are to be considered:

1. Prepare for the tests at UDSM by learn how to calibrate the necessary instruments
2. Participate in finishing the test rig and install measuring equipment at UDSM
3. Perform tests to establish both turbine characteristics and efficiency of the PAT
4. Analyse the results and compere with the mentioned method
5. If the student will go to Nepal for a excursion, earlier and further work will be presented as a publication and presented at the conference; 8^{th} *International symposium on Current Research in Hydraulic Turbines (CRHT-VIII)* at Kathmandu University in March 2018.

-- ” --

Within 14 days of receiving the written text on the master thesis, the candidate shall submit a research plan for his project to the department.

When the thesis is evaluated, emphasis is put on processing of the results, and that they are presented in tabular and/or graphic form in a clear manner, and that they are analyzed carefully.

The thesis should be formulated as a research report with summary both in English and Norwegian, conclusion, literature references, table of contents etc. During the preparation of the text, the candidate should make an effort to produce a well-structured and easily readable report. In order to ease the evaluation of the thesis, it is important that the cross-references are correct. In the making of the report, strong emphasis should be placed on both a thorough discussion of the results and an orderly presentation.

The candidate is requested to initiate and keep close contact with his/her academic supervisor(s) throughout the working period. The candidate must follow the rules and regulations of NTNU as well as passive directions given by the Department of Energy and Process Engineering.

Risk assessment of the candidate's work shall be carried out according to the department's procedures. The risk assessment must be documented and included as part of the final report. Events related to the candidate's work adversely affecting the health, safety or security, must be documented and included as part of the final report. If the documentation on risk assessment represents a large number of pages, the full version is to be submitted electronically to the supervisor and an excerpt is included in the report.

Pursuant to “Regulations concerning the supplementary provisions to the technology study program/Master of Science” at NTNU §20, the Department reserves the permission to utilize all the results and data for teaching and research purposes as well as in future publications.

The final report is to be submitted digitally in DAIM. An executive summary of the thesis including title, student’s name, supervisor's name, year, department name, and NTNU's logo and name, shall be submitted to the department as a separate pdf file. Based on an agreement with the supervisor, the final report and other material and documents may be given to the supervisor in digital format.

☒ Work to be done in lab (Water power lab, Fluids engineering lab, Thermal engineering lab)
☒ Field work

Department of Energy and Process Engineering, 15. January 2018

Torbjørn K. Nielsen
Academic Supervisor

Research Advisor: Mdee Ombeni, UDSM

NTNU
Norwegian University
of Science and Technology

Department of Energy
and Process Engineering

EPT-M-2018-85

MASTER THESIS

for

Student Sondre Skjoldli

Spring 2018

Pump as Turbine (PAT)

Pumpe som turbin (PAT)

Background and objective

For small hydro power plants, both in Norway and in developing countries, the issue is to reduce the turbine price as far as possible. Efficiency has not necessary the highest priority. A centrifugal pump run in reverse is good choice. It has relative good efficiency, it is a robust construction and much cheaper than a turbine. The main reason for the low price is that pumps are mas-produced and there is no wicket gate. The problem is to pick the right pump for given Head and Flow.

We have a PhD student at University of Dar es Salam (UDSM) working on PAT supported by a Norad program (EnPe), and we would like the Norwegian student to be collaborating with him and, if possible, perform tests at Dar es Salam University.

The objective is to veryfy the method described in the Project Work of how to predict the performance of a pump when running as turbine.

The project shall be done in cooperation with stud Øyvind Albert

The following tasks are to be considered:

1. Prepare for the tests at UDSM by learn how to calibrate the necessary instruments
2. Participate in finishing the test and install measuring equipment at UDSM
3. Perform tests to establish both turbine characteristics and efficiency of the PAT
4. Analyse the results and compere with the mentioned method
5. If the student will go to Nepal for a excursion, earlier and further work will be presented as a publication and presented at the conference; 8th *International symposium on Current Research in Hydraulic Turbines (CRHT-VIII)* at Kathmandu University in March 2018.

-- " --

Within 14 days of receiving the written text on the master thesis, the candidate shall submit a research plan for his project to the department.

When the thesis is evaluated, emphasis is put on processing of the results, and that they are presented in tabular and/or graphic form in a clear manner, and that they are analyzed carefully.

The thesis should be formulated as a research report with summary both in English and Norwegian, conclusion, literature references, table of contents etc. During the preparation of the text, the candidate should make an effort to produce a well-structured and easily readable report. In order to ease the evaluation of the thesis, it is important that the cross-references are correct. In the making of the report, strong emphasis should be placed on both a thorough discussion of the results and an orderly presentation.

The candidate is requested to initiate and keep close contact with his/her academic supervisor(s) throughout the working period. The candidate must follow the rules and regulations of NTNU as well as passive directions given by the Department of Energy and Process Engineering.

Risk assessment of the candidate's work shall be carried out according to the department's procedures. The risk assessment must be documented and included as part of the final report. Events related to the candidate's work adversely affecting the health, safety or security, must be documented and included as part of the final report. If the documentation on risk assessment represents a large number of pages, the full version is to be submitted electronically to the supervisor and an excerpt is included in the report.

Pursuant to "Regulations concerning the supplementary provisions to the technology study program/Master of Science" at NTNU §20, the Department reserves the permission to utilize all the results and data for teaching and research purposes as well as in future publications.

The final report is to be submitted digitally in DAIM. An executive summary of the thesis including title, student's name, supervisor's name, year, department name, and NTNU's logo and name, shall be submitted to the department as a separate pdf file. Based on an agreement with the supervisor, the final report and other material and documents may be given to the supervisor in digital format.

☐ Work to be done in lab (Water power lab, Fluids engineering lab, Thermal engineering lab)
☒ Field work

Department of Energy and Process Engineering, 15. January 2018

Torbjørn K. Nielsen
Academic Supervisor

Research Advisor: Mdee Ombeni, UDSM

Preface and acknowledgements

The following Master's thesis has been carried out in the spring of 2018, and the work has been done for the Waterpower Laboratory at the Norwegian University of Science and Technology (NTNU). The project is also a collaboration with a Norad supported program for *Pumps as Turbines*.

The authors would like to thank supervisor Torbjørn K. Nielsen for his valuable help and guidance throughout the project, as well as the laboratory technicians for their countless efforts. Additionally, Ph.D. candidate Carl W. Bergan has provided us with significant aid during the experiments and testing procedure. Furthermore, we would like to thank co-supervisor Mdee Ombeni for his contribution, as well as the technicians at the University of Dar es Salaam (UDSM), Tanzania.

Trondheim, 2018-06-11

Øyvind Albert and Sondre Skjoldli

Abstract

As a cheap and available source of renewable energy, regular centrifugal pumps may be run in reverse to act as hydro turbines. Pumps as turbines (PAT) are especially relevant for isolated rural areas, or in developing countries, where efficiency is not necessarily the highest priority. The main challenge, however, is to be able to pick a suitable pump for a given site, which coincides with the available head and discharge. In order to make this decision, one has to be able to predict how a certain pump will perform as a turbine. A lot of work has been done in the past to establish such prediction methods, based on tests and empirical correlations. Many of these methods only predict one optimal point of operation, but as pumps do not have any guide vanes, it will be difficult to constantly operate a PAT at this specific point. Therefore, this may be insufficient. With this in mind, and because of the inaccuracies of these methods, a new approach has been suggested - an approach in which full head-flow characteristics are predicted based solely on the pump's impeller geometry.

By assuming symmetry in the velocity diagrams of pump and turbine operation, a method for establishing the PAT characteristic was made. For validation purposes, this method was applied to one specific pump. Experimental results revealed a slight asymmetry, and shortcomings in the initial assumptions. Therefore, the model was modified thereafter, with the introduction of an empirical constant. The predicted characteristic lacks some accuracy in comparison to the real PAT characteristic found through testing, but its optimal point of operation is in line with previous established prediction methods. Still, the modifications, and the empirical constant, may be enhanced further through comprehensive testing of numerous pumps, of various type.

Sammendrag

Som en billig og tilgjengelig fornybar energikilde, kan vanlige sentrifugalpumper brukes som vannkraftturbiner. Å bruke en pumpe som turbin (PAT) er spesielt relevant for avsidesliggende områder, og utviklingsland, hvor turbinens effektivitet ikke nødvendigvis er av høyeste prioritet. Hovedutfordringen ligger i å velge riktig pumpe for et gitt anlegg, som sammenfaller med områdets vannføring og trykk. For å kunne ta denne avgjørelsen, må man kunne forutsi hvordan en spesifikk pumpe vil prestere som en turbin. Det er tidligere gjort mye arbeid for å etablere slike predikasjonsmetoder, basert på tester og empiri. Mange av disse metodene predikerer kun et optimalt driftspunkt, men ettersom pumper ikke har justerbare ledeskovler, er det vanskelig å operere en PAT i dette ene punktet. De kan derfor vise seg å være utilstrekkelige. På grunn av dette, samt unøyaktighetene knyttet til disse metodene, har det blitt foreslått en ny fremgangsmåte - en metode som predikerer en full turbinkarakteristikk basert på geometrien til pumpens løpehjul.

Ved å anta symmetri mellom hastighetsdiagrammene i pumpe- og turbindrift, har en modell blitt etablert for predikere PAT-karakteristikken. For å validere metoden, har den blitt anvendt på en spesifikk pumpe. Eksperimentelle resultater avslørte en viss asymmetri, og mangler i de initielle antagelsene. Modellen ble modifisert deretter, og en empirisk konstant ble introdusert. Sammenlignet med den reelle test-karakteristikken, er den predikerte karakteristikken noe unøyaktig. Likevel er det estimerte optimale driftspunktet i tråd med tidligere etablerte predikasjonsmetoder. Modifikasjonene, og den empiriske konstanten, kan imidlertid blir videre forbedret gjennom testing av flere ulike pumper.

List of Tables

2.1 Different prediction methods investigated by Williams (1994)[1]. 7

3.1 Test-Pump 2 impeller geometry. 18
3.2 Pump impeller geometry and rotational speed of Pedrollo FG 32/160B. 22
3.3 Total uncertainty for the experiment parameters. 27

4.1 Comparison of test and estimated values in pump operation. 31
4.2 Comparison of PAT parameters - tests and predictions. 36

B.1 Component errors in the calibration of an instrument. 63
B.2 Calibration uncertainties for pressure transducer upstream of the PAT. 64
B.3 Calibration uncertainties for pressure transducer downstream of the PAT. 64
B.4 Calibration uncertainties of the flow sensor. 65
B.5 Calibration uncertainties for the torque sensor in both pump and turbine operation. 66

List of Figures

2.1 A centrifugal pump operating in a) pump mode and b) turbine mode [2]. 4
2.2 Typical performance curves of pumps and turbines, adapted from [3]. 9
2.3 Illustration of the phenomenon presented by Jain and Patel (2013)[2]. 10
2.4 Obtaining the PAT velocity diagrams by symmetry (not to scale). 11

3.1 PAT test set-up UDSM. 18
3.2 PAT test rig at UDSM: Water enters the PAT from the left in the picture, and exits in the foreground. To the right the shaft goes from the PAT to the generator, with a torque transducer in between. 19
3.3 a) Insertion of permanent magnets into the rotor - b) stator. 20
3.4 The pump impeller of Pedrollo FG 32/160B. 22
3.5 Illustration of test rig constructed at NTNU, designed in Creo. 24

4.1 $H-Q$ characteristic and efficiency curve from pump testing. 30
4.2 $H-Q$ characteristics, both predicted and acquired through testing. 32
4.3 Pump as turbine efficiency curve. 33
4.4 Velocity diagrams from test results. 34
4.5 $H-Q$ characteristics, improved predicted curves and the one acquired through testing. 36

Nomenclature

Acronyms

BEP	Best Efficiency Point
CFD	Computational Fluid Dynamics
PAT	Pump As Turbine

Greek Symbols

α	Angle between absolute velocity and peripheral velocity	°
β	Impeller blade angle	°
η	Efficiency	
κ	Guide vane opening degree	
ω	Angular velocity	rad/s
ψ	Machine coefficient	
ρ	Density	kg/m^3
σ	Dimensionless throttling dependency of angular speed of rotation	
τ	Torque	Nm
$\tilde{\omega}$	Dimensionless angular velocity	

Roman Symbols

$\tilde{h}$	Head correction factor	
$\tilde{q}$	Discharge correction factor	
A	Cross-sectional area	m^2
B	Impeller height	m
c	Absolute velocity	m/s

D	Diameter	m
g	Gravitational acceleration	m/s^2
H	Head	m
h	Dimensionless head	
k	Empirical constant	
n	Rotational speed	rpm
N_s	Specific speed	
n_{ed}	Speed factor	
P	Power	W
p	Pressure	Pa
Q	Discharge	m^3/s
q	Dimensionless discharge	
Q_{ed}	Discharge factor	
t	Time	s
T_{wt}	Time constant representing hydraulic inertia	s
u	Peripheral velocity	m/s
v	Relative velocity	m/s
Z	Height	m

Subscripts

1	Runner inlet
2	Runner outlet
bep	Best efficiency point value
h	Hydraulic
in	Refers to the inlet
m	Meridional component
out	Refers to the outlet
p	Refers to pump operation
R	Rated value
t	Refers to turbine operation
u	Tangential component

Contents

Preface and acknowledgements v
Abstract vi
Sammendrag vii
List of tables vii
List of figures ix
Nomenclature x

1 Introduction **1**

2 Theoretical background **3**
2.1 The concept of a Pump as Turbine 3
2.1.1 Advantages and disadvantages of a PAT 4
2.2 Earlier work 6
2.3 Pump and turbine performance 8
2.4 Symmetry method 10
2.4.1 Design equations and assumptions 12
2.4.2 Producing the PAT's $H-Q$ curve 13
2.5 Experimental preparation 14

3 Methodology **17**

3.1 Experimental setup UDSM 17

3.2 Pedrollo FG 32/160B 21

3.3 Experimental setup NTNU 22

3.4 Data acquisition 24

3.4.1 Pump operation 24

3.4.2 Pump as Turbine 26

3.5 Calibration and uncertainty 26

4 Results **29**

4.1 Pump testing 29

4.2 PAT testing 31

4.2.1 Velocity diagrams 33

4.3 Potential improvements 35

5 Discussion **37**

5.1 Pump testing 37

5.2 PAT testing 38

5.2.1 First modification 39

5.2.2 Second modification 40

5.2.3 Assumptions and inaccuracies 40

5.2.4 Additional challenges and further work 42

6 Conclusion **43**

Bibliography **45**

A Paper written for CRHTVIII'18 **47**

B Calibration and Uncertainty Analysis **63**

B.1 Pressure sensors 64

B.2 Flow sensor 65

B.3 Torque sensor 65

B.4 RPM sensor . . . 66
B.5 Temperature sensor . . . 66
B.6 Uncertainty of derived values . . . 66
B.6.1 Pressure head . . . 67
B.6.2 Efficiency . . . 68
B.7 Uncertainty from measurements . . . 69
B.8 Calibration certificates . . . 70
B.8.1 Calibration certificate Druck DPI601 . . . 70
B.8.2 Calibration certificate OPTIFLUX 2000 C . . . 71
B.8.3 Calibration certificate Druck PTX 1400 . . . 72
B.8.4 Calibration certificate GE UNIK 5000 . . . 73
B.8.5 Calibration certificate HBM T22 for pump operation . . . 74
B.8.6 Calibration certificate HBM T22 for turbine operation . . . 75

C LabVIEW **77**
C.1 Front panel and block diagram . . . 78

D Matlab codes **81**
D.1 PAT prediction and experimental results compared . . . 81
D.2 Pump experimental results . . . 87
D.3 Test velocity diagrams . . . 90
D.4 Error function . . . 92

E Risk assessment **93**

CHAPTER 1

Introduction

Micro-hydropower has a great potential, and can be very beneficial in order to help electrify isolated communities, with no connection to the power grid. This can especially be relevant in developing countries, small villages, and hilly rural areas. Even though running costs of such plants are low and affordable, the biggest hurdle to some of these communities is the high initial investment cost [4]. One appropriate solution is to use a pump as a turbine (PAT), where a regular centrifugal pump will be able to generate energy by being run in reverse.

Pumps are significantly cheaper than regular hydro turbines, they are simple and robust machines, and easily available throughout the world. Also, because they are more widespread, spare parts and qualified personnel to conduct repairs are also more available [5]. However, the main challenge of installing a PAT is the difficulty of predicting how a certain pump will perform as a turbine. Determining this performance is crucial, because unlike a turbine, a centrifugal pump does not have any adjustable guide vanes. Therefore, if the running speed is fixed, a PAT is only able to perform efficiently for one set of head and flow values [1]. In consequence, it is critical to be able to pick a pump that correlates with the available head and discharge at the planned PAT site.

Some researchers have developed prediction methods that relate the best efficiency point

(BEP) in pump operation to the one in PAT operation. However, it has been shown that these empirical methods deviate by ±20% from experimental data [5]. In recent years, attempts of predicting the pump as turbine performance have been made through computational fluid dynamics (CFD). Still, these results are not reliable unless they are verified against experimental data. This has motivated a new approach, an approach in which the PAT performance is estimated based on the pump's impeller geometry.

This proposed prediction method is based on assuming symmetry in the velocity diagrams of pump and turbine operation. Even though a slight asymmetry might be expected, its impact is presumed to be low. However, this may be accounted for postliminary. Additionally, it differs from many of the old empirical correlations, in the way that it predicts a full head-flow ($H-Q$) characteristic, instead of only one best efficiency point. This is especially important, as it is hard to constantly operate a PAT at its BEP. In order to optimize PAT usage an accurate prediction model is necessary. The goal is therefore to verify the symmetry prediction method presented, and to investigate the method's validity. This will be done through experimental PAT tests in the laboratory.

CHAPTER 2

Theoretical background

Some parts of the following section was developed for the paper *Symmetry prediction method for pump as turbine characteristics* and presented at the 8th edition of the annual *Symposium on Current Research in Hydraulic Turbines (CRHTVIII'18)* at Kathmandu University in March of 2018. However, the authors feel this is material which is necessary to present again, in order to fully comprehend the concept of a PAT, as well as the developed PAT prediction method. The paper may be read in full in appendix A.

2.1 The concept of a Pump as Turbine

In a time where renewable power production is becoming increasingly important, the motivation to reduce the costs as far as possible also gets a lot of attention. One appropriate technology is to use a pump as a turbine. This will include using a regular centrifugal pump, and running it in reverse, as illustrated in figure 2.1. In that way, one will be able to extract energy from a fluid instead of putting energy into it. The idea is not at all new, but could prove to be increasingly relevant and important for developing countries, and isolated rural areas, where the electricity demand is ever growing [2].

Even though operational and running costs of a hydropower plant are low and affordable, the high initial capital cost in the development of such a plant can truly be a barrier [4]. Additionally, as large-scale generation is not always feasible, there is an increasing interest in small-scale hydropower plants. In these small-scale plants, it can often be hard to justify the construction costs in comparison to the total power generation possible [6]. It is in these situations a PAT can show its full potential, and can prove to be a very suitable technology, because of its low price. The price per kW produced by small-scale hydropower plants, are usually higher than that of large hydropower plants [2]. Therefore, installment of a PAT could be essential in reducing these costs.

Unlike hydraulic turbines, centrifugal pumps are mass produced, which in turn make them a lot more economically viable. However, the solution is mostly relevant for power plants where the efficiency is not of the highest priority, as a pump run in reverse never will achieve efficiencies of the same order as a turbine designed for specific conditions [2].

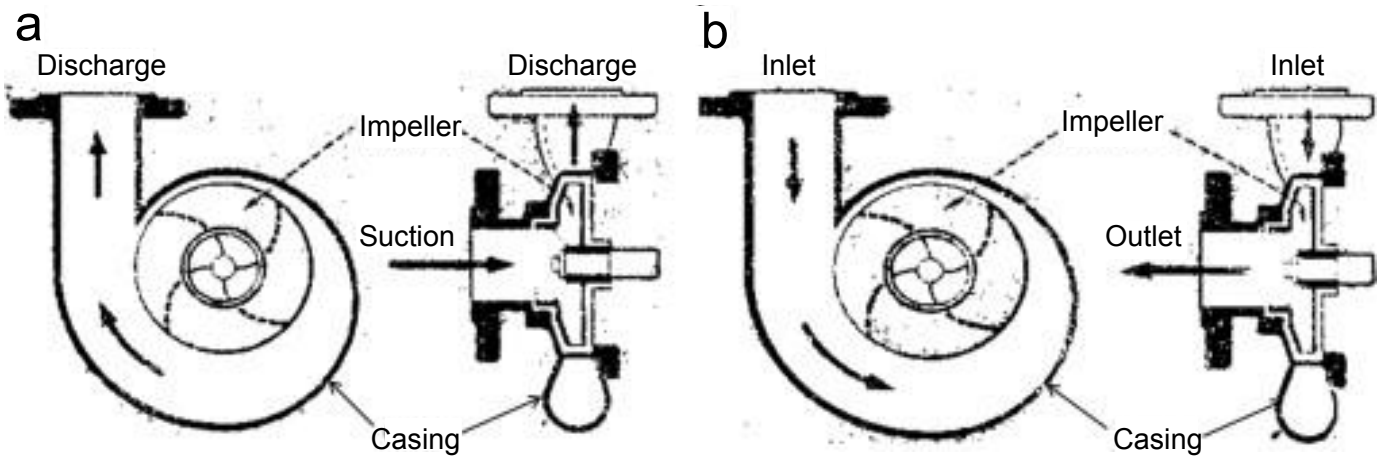

Figure 2.1: A centrifugal pump operating in a) pump mode and b) turbine mode [2].

2.1.1 Advantages and disadvantages of a PAT

If a centrifugal pump is to be used as a PAT, the advantages and disadvantages have to be carefully weighed up against each other. From an economic investment point of view, PATs have a clear advantage, as centrifugal pumps are mass produced all over the world, and are manufactured for a wide range of heads and flows. By being able to pick a centrifugal pump right off the shelf, a PAT will be a significantly cheaper option than a turbine designed for specific con-

ditions. In other words, they are more accessible and investments costs are lower. What's more is that they are easy to install, easy to maintain, and that spare parts are easily available [4]. As pumps are a more widespread technology than turbines, qualified people to conduct repairs and maintenance are also more available.

It has been shown that in low capacity power plants, up to 500 kW, installment of a PAT may reduce the capital costs by the order of 10-1, compared to a conventional hydro turbine [6]. As investment costs of hydro turbines in this range often can be quite high, the payback period can be reduced from as much as 15 years to 2 years, if a PAT is installed instead [2].

Additionally, the pump with its integrated motor may be used as a turbine and generator set. Thus, instead of buying an expensive synchronous generator, one may apply the provided induction motor as an asynchronous generator [4].

There are several disadvantages however. Even though Fernandez et al. (2004)[6] state that the efficiency of a pump running in reverse has almost the same efficiency as in pump mode, it will most certainly not perform as well as a custom made turbine. It may seem as if the pump industry is not as concerned as the turbine industry, with gaining the highest efficiency possible. Whereas a hydro turbine has a very smooth surface to minimize losses, a mass produced pump will often have a high level of roughness on the impeller. Even though it may be cumbersome, manual grinding and smoothing of the PAT's impeller may prove advantageous and worthwhile.

Moreover, pumps experience the highest pressure at their discharge, where turbines experience the highest pressure at the intake. The seals in both pumps and turbines are designed for a specific expected pressure distribution [7]. However, the pressure build-up the pump is designed for does not necessarily equal the pressure drop when using it as a turbine. It is possible that at the PAT outlet, some points will experience higher pressures than those for which the seals were designed for. If so, the seal must be redesigned or reinforced at these points.

Another key thing is that a centrifugal pump, compared to a regular hydro turbine, does not have any guide vanes. Guide vanes are a number of blades that can be adjusted in order to increase or decrease the flow rate through the turbine [8]. The vanes are placed between two parallel covers normal to the turbine shaft. Pumps do not have such guide vanes, meaning they cannot control the flow in the same way as turbines. Whereas a regular hydro turbine can adjust incoming flow, and is able to perform efficiently for a range of flow rates, a PAT does not have

this option [9]. This will enable regular hydro turbines to produce power at BEP, even through varying conditions. By implication, the range of suitable operating flow rates is much more limited for a PAT. One solution to this problem is to have multiple PATs coupled in parallel. With such a rig, one will be able to activate the number of pumps required to handle the incoming flow rate most efficiently. Having said that, a single PAT may perform close to maximum efficiency if a suitable pump is chosen for the given site conditions. Especially if the site has a close to fixed water supply throughout the year.

The primary disadvantage of a PAT however, is the difficulty of predicting how a certain pump will behave as a turbine [4]. Thus, if a centrifugal pump is to be picked right off the shelf, one has to be able to accurately predict its performance. The main challenge therefore lies in being able to pick a suitable pump for a given site, which has a turbine characteristic that coincides with the available head and discharge. A lot of work has been done in the past to establish such prediction methods, based on tests and empirical correlations.

2.2 Earlier work

As the main disadvantage of a PAT is the difficulty of predicting the turbine characteristics that are needed for a given site, a lot of work has been done throughout the years to establish prediction methods which calculates the performance [1]. The actual turbine performance must be found through testing, but this is a costly and time consuming process, as well as it requires that the pump has already been purchased. Therefore, many different empirical correlations have been produced, which in turn produce a wide range of results. A common factor, however, is that the optimal operating point of a PAT is higher in both head and flow, than that of the pump it originates from [2]. This is to account for the head reduction caused by the different losses. In recent years, turbine performance have been predicted through CFD, but these results are not reliable unless they are verified against experimental data [5].

The two main empirical approaches that have been taken to predict turbine performance are either by relating the head and flow ratios to the pump's efficiency, or by using its specific speed [1]. Williams (1994)[1] investigated in total eight different prediction techniques, and compared the accuracy of the models. Table 2.1 gives an outline of the different methods, as well as the

appropriate relationship of the head correction factor $\tilde{h} = \frac{H_t}{H_p}$ and the discharge correction factor $\tilde{q} = \frac{Q_t}{Q_p}$.

Table 2.1: Different prediction methods investigated by Williams (1994)[1].

Name of method/investigator	Based on	Head correction factor $\tilde{h}$	Discharge correction factor $\tilde{q}$
Childs	BEP	$\frac{1}{\eta_p}$	$\frac{1}{\eta_p}$
Hancock	BEP	$\frac{1}{\eta_t}$	$\frac{1}{\eta_t}$
Stepanoff	BEP	$\frac{1}{\eta_p}$	$\frac{1}{\sqrt{\eta_p}}$
Sharma	BEP	$\frac{1}{\eta_p^{1.2}}$	$\frac{1}{\eta_p^{0.8}}$
Alatorre-Frenk	BEP	$\frac{1}{0.85\eta_p^5+0.385}$	$\frac{0.85\eta_p^5+0.385}{2\eta_p^{9.5}+0.205}$
Schmiedl	BEP	$-1.4+\frac{2.5}{\eta_{hp}}$	$-1.5+\frac{2.4}{\eta_{hp}^2}$
Grover	Specific speed	$2.693-0.0229N_{st}$	$2.379-0.0264N_{st}$
Hergt	Specific speed	$1.3-\frac{6}{N_{st}-3}$	$1.3-\frac{1.6}{N_{st}-5}$

According to Williams' study, the method of Sharma proved to be the most accurate one. The study involved comparing the turbine prediction methods on 35 different pumps, with available test data. As Sharma's method proved to be the most accurate, it is the only one that will be looked at here. He relates the discharge and head correction factors to the pump efficiency as shown in equations 2.1 and 2.2, where H and Q is the best efficiency point values of head and discharge, and subscripts p and t refer to pump and turbine mode, respectively.

$$\tilde{q} = \frac{Q_t}{Q_p} = \frac{1}{\eta_p^{0.8}} \tag{2.1}$$

$$\tilde{h} = \frac{H_t}{H_p} = \frac{1}{\eta_p^{1.2}} \tag{2.2}$$

Even though a few of the other methods proved competitive, Sharma's method was found

to be the most accurate of the eight approaches. Still, 20 percent of the tested pumps fell outside what was said to be the "acceptable" prediction limits. Therefore, it will always be wise to conduct thorough tests before installing a certain PAT [1].

Although the accuracy of the different correlations can be questioned, they may serve as a rough guide when designing a PAT-site [10]. However, the questionable precision, along with the large number of different pumps that need to be tested to create a trustworthy model, motivates a new approach. An approach in which the turbine performance is determined solely based on the pump's geometry. Additionally, common for the eight different prediction models in table 2.1 is that they only predict one set of BEP values. They do not provide any answer of how head and flow are related on either side of this point. As stated previously, because of the lack of guide vanes, it will be more challenging to operate a PAT at its best efficiency point, than for a turbine. Therefore, developing a new method that predicts a full turbine characteristic may truly prove advantageous.

2.3 Pump and turbine performance

Figure 2.2 shows typical performance characteristics of pumps and turbines at constant rotational speed. It describes the variation of flow with head, power and efficiency. As seen from the graph to the left in the figure, the pump height decreases with increasing volume flow. In turbine operation this relationship is reversed, where both variables are strictly rising. The highest value of η indicates where the location of the best efficiency points are found in both modes. This is the desired point of operation, and is described by H_{bep} and Q_{bep}.

The P-curve shows typical power distributions for different flow rates. In pump operation this line represents consumed power, while in turbine mode power is generated. The power curve of the turbine naturally increases for increased head and flow, but the maximum efficiency is not necessary where the power is at its maximum.

When operating a pump as a turbine it can be expected that the $H-Q$ curve in turbine mode is similar to that of a regular turbine [9]. Therefore, this curve is relevant and comparable when considering the validity of the following PAT experiments.

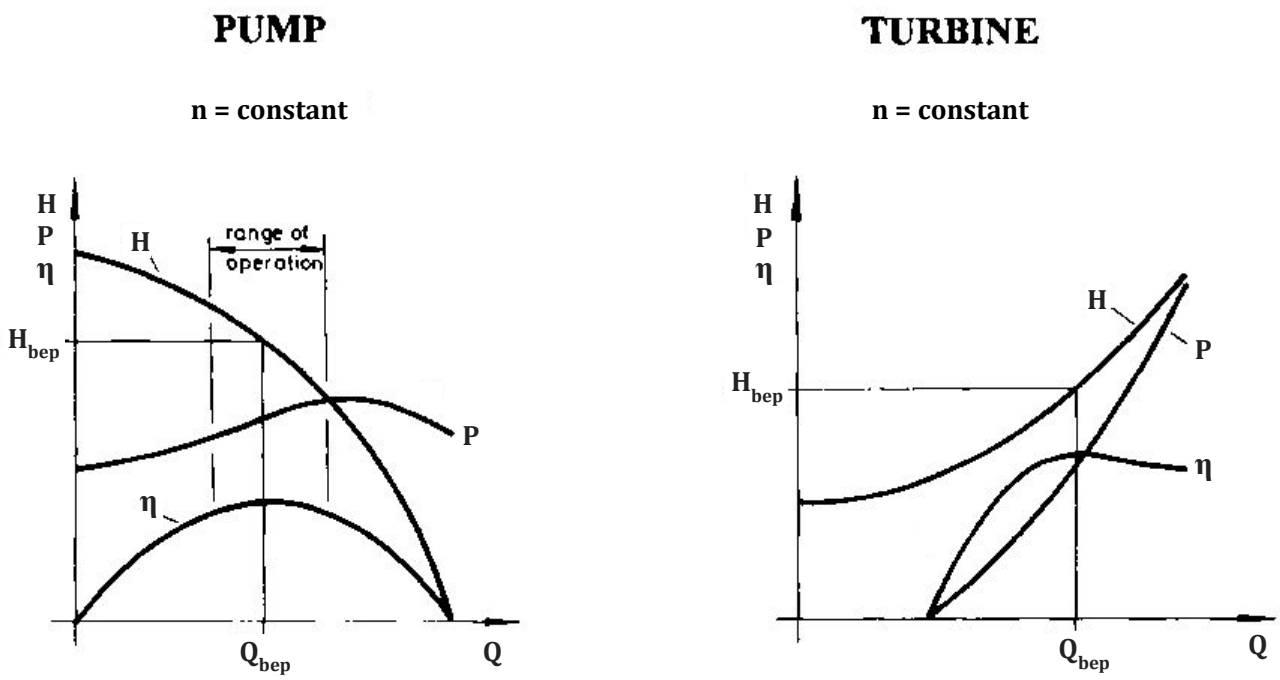

Figure 2.2: Typical performance curves of pumps and turbines, adapted from [3].

Another interesting aspect to note when investigating a pump running as a turbine, is what was presented by Jain and Patel (2013)[2]. Figure 2.3 shows the characteristics of a PAT in both pump and turbine mode, labelled with positive and negative flow rates, respectively. It also includes the different losses a pump and turbine are subjected to. It was found that at zero flow, and at constant but opposite rotational speed, there is a difference in pressure head between the two operations. This gap is represented by the red line in figure 2.3. Intuitively, one would expect these two characteristics to intersect at the ordinate axis, at the same head. However, the magnitude of the various losses in turbine and pump mode are not necessarily equal, which could be a reason for the head difference. This phenomenon could also have a meaningful impact when trying to predict the transition from pump to turbine operation.

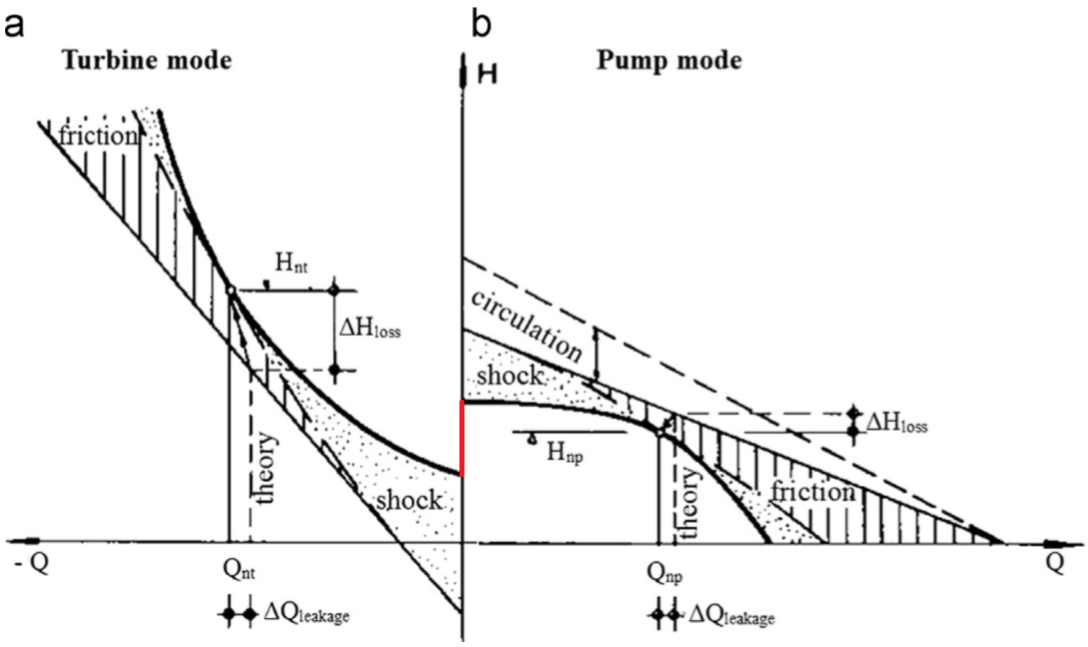

Figure 2.3: Illustration of the phenomenon presented by Jain and Patel (2013) [2].

2.4 Symmetry method

As described previously, the main challenge of a PAT is to predict the performance of a specific pump in turbine mode. The prediction method presented here is based on assuming symmetry in the velocity diagrams from pump and turbine operation. By this assumption, the inlet diagram of a turbine can be directly mirrored from the outlet diagram of a pump. The same procedure can then also be applied to find the turbine outlet diagram, from the pump inlet diagram. In reality, the optimal operating point in PAT operation is anticipated to lie higher than in pump operation, as already mentioned. Thus, a slight asymmetrical relationship might be expected. Still, symmetry is the initial assumption, as the asymmetry is expected to have a limited impact on the prediction. However, if experiments prove otherwise, this can be accounted for accordingly.

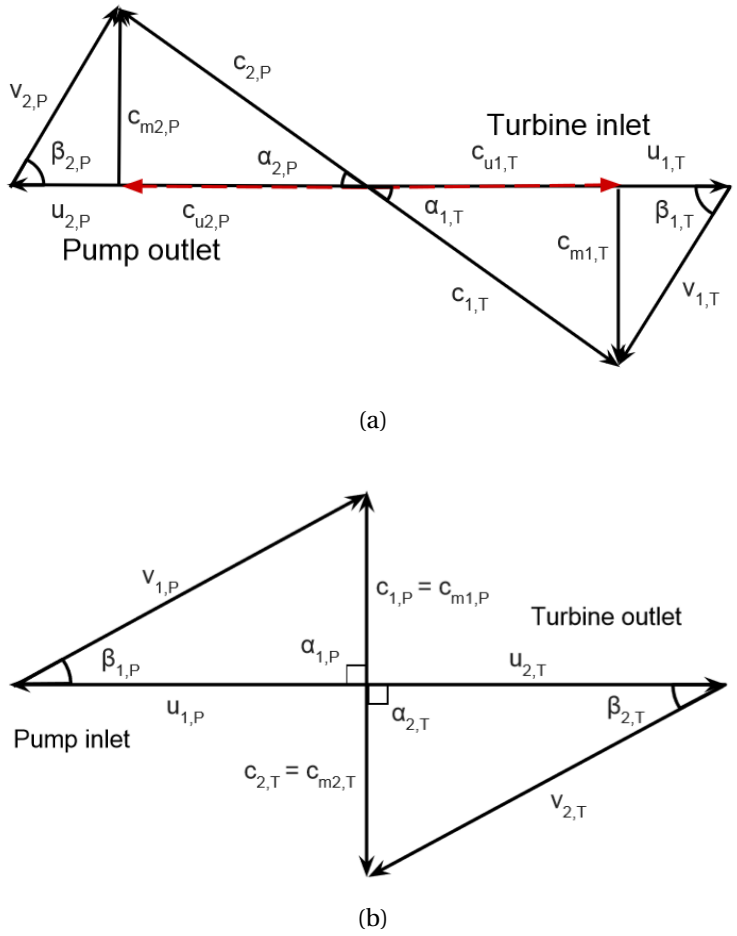

Figure 2.4: Obtaining the PAT velocity diagrams by symmetry (not to scale).

The two respective diagrams and their mirrored opposites are presented in figure 2.4a and 2.4b. It is important to note that with this approach the slip and losses, such as friction and shock losses, are not directly accounted for. Slip would have altered the blade angle to the relative flow angle, and consequently changed the velocity diagram in turbine mode. The omitting of the slip however, may be justified as the effect of slip in turbine operation, compared to pump operation, will be modest [3]. This, and further losses, will be a topic of discussion later.

Different from the methods presented previously, the symmetry method is not based on either pump efficiency or specific speed. As it is solely dependent on the pump geometry, it requires physical measurement of the impeller to acquire the necessary input. This is because the impeller geometry data is seldom published by pump manufacturers. The necessary parameters consist of inlet and outlet diameter, inlet and outlet height, and outlet blade angle. Also,

the rotational speed is needed, as well as an assumption of the inlet meridional velocity - an assumption which also will be subjected to further discussion later on. From this, the BEP values of head and flow for a pump running as a turbine can be calculated through trigonometry and standard hydropower design equations.

2.4.1 Design equations and assumptions

As the prediction method is based on a symmetrical transition between parameters in pump and turbine mode, it requires determination of the different velocity components, as well as head and flow at the best efficiency point. These are calculated through trigonometry and standard turbine design equations, as presented by Brekke (2003)[11]. Firstly, the peripheral velocity is found as $u = \omega r$, where ω is the angular velocity, and r the radius. Then, the pump's inlet meridional velocity component at BEP, $c_{m1,p}$, is assumed based on numbers given by Bye (1967)[12]. This is an assumption which will be discussed in great detail later on. From this, and because the β-angles in the geometry is already known, the other parameters in the velocity triangle are calculated.

Further, a 10% acceleration is assumed through the runner in pump operation. Hence $c_{m2,p} = 1.1c_{m1,p}$. Then, when symmetry is applied to the velocity components in pump mode, the relationship is reversed, and turns to $c_{m1,t} = 1.1c_{m2,t}$.

To be able to predict the rated flow at a certain PAT's best efficiency point, the meridional velocity component, along with the cross-sectional area, gives an estimate through conservation of mass. To predict the rated head, Euler's equations may be applied. Euler's pump and turbine equations are defined as follows:

$$\eta_{h,p} = \frac{gH_p}{u_{2,p}c_{u2,p} - u_{1,p}c_{u1,p}} \tag{2.3}$$

$$\eta_{h,t} = \frac{u_{1,t}c_{u1,t} - u_{2,t}c_{u2,t}}{gH_t} \tag{2.4}$$

Where η_h is the hydraulic efficiency, g is the acceleration due to gravity, and c_u is the tangential component of the absolute velocity.

Another assumption worth noting is the assumption of no rotation at the inlet of the pump

and the outlet of the PAT. With this swirl free assumption, equations 2.3 and 2.4 simplifies as $c_{u1,p} = 0$ and $c_{u2,t} = 0$ [11]. Also, the symmetry method assumes a rather bold hydraulic pump efficiency of $\eta_{h,p} = 1$ in determination of the velocity components. This is also an assumption which will be subjected to discussion in due time.

2.4.2 Producing the PAT's $H - Q$ curve

Up until now it is only the performance at the best efficiency point that has been addressed. However, it is very much of interest to be able to predict how the PAT will perform at either side of this point, as BEP operation is hard to maintain for a PAT with no guide vanes. This is possible by manipulating the dimensionless momentum equation presented by Nielsen (2015)[13]:

$$T_{wt}\frac{dq}{dt} = h - \frac{q|q|}{\kappa^2} - \sigma(\tilde{\omega}^2 - 1) = 0 \tag{2.5}$$

where T_{wt} is a time constant representing the hydraulic inertia. This value is not needed however, as the left hand side of the equation can be set to zero to find the stationary characteristic. Furthermore, the dimensionless properties for flow, head and angular speed of rotation in equation 2.5 are defined as $q = Q_t/Q_{R,t}$, $h = H_t/H_{R,t}$ and $\tilde{\omega} = \omega/\omega_R$. Now, it can be assumed that the PAT has its BEP at $q = 1$, $h = 1$, $\tilde{\omega} = 1$, and that the derivative of the hydraulic efficiency in Euler's turbine equation (2.4) with regards to ω is zero, $\partial\eta/\partial\omega = 0$. In that way, the PAT's dimensionless throttling dependency of angular speed of rotation, σ, is defined as follows:

$$\sigma = \frac{\eta_{hR} - \psi}{\eta_{hR} + \psi} \tag{2.6}$$

By setting the hydraulic efficiency, $\eta_{hR} = 1$ for the BEP in equation 2.6, and defining the machine coefficient as

$$\psi = \frac{{u_{2,t}}^2}{gH_{R,t}}, \tag{2.7}$$

σ for the PAT can be found. Further, the opening degree of the turbine, κ, equals 1 at the best efficiency point, and is defined as seen in equation 2.8. Q_R is the rated volume flow in the turbine's best efficiency point.

$$\kappa = \frac{\frac{Q_t}{\sqrt{2gH_t}}}{\frac{Q_{R,t}}{\sqrt{2gH_{R,t}}}} \tag{2.8}$$

By varying the rotational speed n, and solving the stationary version of equation 2.5 for q, the discharge Q_t for different rotational speeds can be determined. IEC 62097 [14] specifies the two dimensionless factors for speed and discharge, shown in equation 2.9 and 2.10 respectively.

$$n_{ed} = \frac{nD_{2,t}}{\sqrt{gH_{R,t}}} \tag{2.9}$$

$$Q_{ed} = \frac{Q_t}{D_{2,t}^2\sqrt{gH_{R,t}}} \tag{2.10}$$

From these two equations the turbine's $Q_{ed} - n_{ed}$ relationship can be established. The $H-Q$ curve can then be produced by modifying equations 2.9 and 2.10. H_t is found by keeping the rotational speed constant, and only varying the speed factor. Q_t, on the other hand, is found for changing values of Q_{ed} and corresponding values of H_t. The two final equations, which enables graphing of the turbine's $H-Q$ relationship, are presented in equations 2.11 and 2.12.

$$H_t = \frac{\left(\frac{nD_{2,t}}{n_{ed}}\right)^2}{g} \tag{2.11}$$

$$Q_t = Q_{ed}D_{2,t}^2\sqrt{gH_t} \tag{2.12}$$

2.5 Experimental preparation

The only way to properly validate the aforementioned prediction method, is to conduct thorough tests in the laboratory, where the performance of the PAT is tested for a range of heads and flows. By producing the actual $H-Q$ curve for a pump working in turbine mode, it will be possible to compare the accuracy of the theoretical model to what happens in reality.

There are three essential test variables that are necessary to construct the PAT's $H-Q$ relationship. Head and flow are self explanatory, but the rotational speed is also important to monitor, as it will need to be held constant for one specific $H-Q$ curve. Furthermore, in addition

to validating the prediction model, it will be of great interest to measure the power output, and investigate the actual PAT efficiency. The maximum efficiency is also important to investigate, in order find the head and flow values at the best efficiency point.

In order to calculate the pressure head, Bernoulli's equation (2.13) may be used. In equation 2.13 Δp is the pressure difference, $p_{in} - p_{out}$, ΔZ is the height difference, while A_{in} and A_{out} is the cross-sectional area of these two locations. Further, V is the velocity of the water flow, and ρ is the water density.

$$H = \frac{\Delta p}{\rho g} + \Delta Z + \frac{\Delta V^2}{2g} = \frac{\Delta p}{\rho g} + \Delta Z + \frac{Q^2 \left(\frac{1}{A_{in}^2 - A_{out}^2} \right)}{2g} \tag{2.13}$$

This implies that in order to calculate the head, the pressure at two locations, the inlet and outlet of the PAT, as well as the volume flow Q, is required. Thus, it is essential that the laboratory test rig is equipped with two pressure sensors and a flow meter.

Furthermore, as it is of interest to measure the actual PAT efficiency, another relationship is necessary. The power of the rotating shaft may be expressed as in equation 2.14, where τ is the torque and ω is the angular velocity [11].

$$P = \tau \omega \tag{2.14}$$

Additionally, the power may also be expressed by the use of equation 2.15 for a turbine, and equation 2.16 for a pump. With this, the efficiency, η, of the system can be calculated for both turbine and pump mode as long as the torque, τ, is known. Therefore, it is necessary to mount a torque transducer on the shaft between the pump and electric motor, to register and log the moment of force.

$$P = \eta_t \rho g Q H \tag{2.15}$$

$$P = \frac{\rho g Q H}{\eta_p} \tag{2.16}$$

CHAPTER 3

Methodology

With the purpose of validating the symmetry prediction method, laboratory tests were scheduled to be conducted at the University of Dar es Salaam (UDSM), Tanzania, in January 2018. At UDSM we would aid co-supervisor Mdee Ombeni in preparing a test rig, equip it with the necessary measuring equipment, and obtaining the required data. As previously stated, the PAT's $H-Q$ relationship is of utmost importance for validation purposes, but investigation of the PAT efficiency will also be of interest.

3.1 Experimental setup UDSM

The pump available for PAT testing at UDSM, hereby referred to as *Test-Pump 2*, was an old pump with no known pump characteristics. The first step was to remove the spiral casing, and manually measure the relevant impeller lengths and angles. The important pump dimensions, as well as the operating conditions, are presented in table 3.1.

After that, the plan was to test the pump in PAT operation in a test rig erected by co-supervisor Mdee Ombeni. The test rig was equipped with the necessary instrumentation, and a sketch of the set-up can be seen in figure 3.1. A picture of a portion of the rig can be seen in figure 3.2.

Table 3.1: Test-Pump 2 impeller geometry.

Parameter	Value	Unit
Inlet diameter $D_{1,p}$	164.5	mm
Outlet diameter $D_{2,p}$	200	mm
Inlet height $B_{1,p}$	74	mm
Outlet height $B_{2,p}$	39	mm
Outlet blade angle $\beta_{2,p}$	37.9	°(degrees)
Rotational speed n	1450	rpm

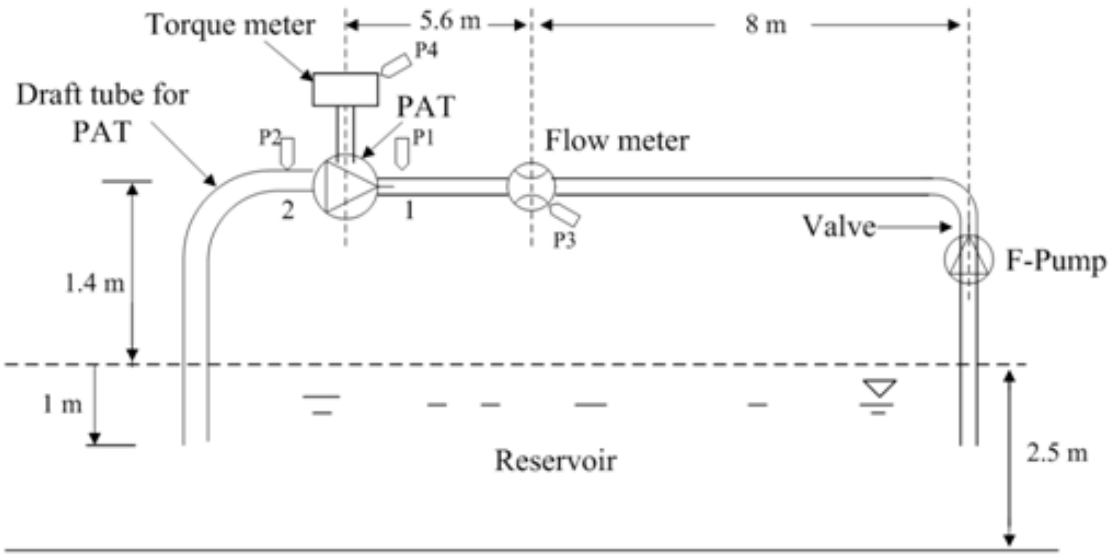

Figure 3.1: PAT test set-up UDSM.

To feed the PAT, a pump designed for flow $Q = 350m^3/h$ and head $H = 10m$ was used. This is what is labeled as *F-Pump* in figure 3.1. It has been estimated that the feed pump will need approximately four times the power rating of the PAT, to be able to produce heads and flows high enough above the BEP [9].

Moreover, pressure sensors were mounted on both the high and low pressure side of the PAT, labelled *P1* and *P2* respectively. However, the possibility of calibrating the equipment was somehow inadequate. For the pressure transducers, UDSM had access to a pressure calibration unit, but at the time of our visit this piece of equipment was faulty. Hence, the manufacturer's calibration had to be trusted initially. The flow meter was located in the horizontal pipe section between the feed pump and the PAT. This sensor was not re-calibrated either, and will not be

until UDSM receives the necessary calibration apparatus.

Figure 3.2: PAT test rig at UDSM: Water enters the PAT from the left in the picture, and exits in the foreground. To the right the shaft goes from the PAT to the generator, with a torque transducer in between.

Further, the torque transducer was mounted on the shaft between the PAT and the generator. In the absence of essential equipment to calibrate this, one would again have to rely on the manufacturer's calibration, for the time being. Also mounted on the shaft was a small piece of reflector tape, in order to keep track of the rotational speed. As it is of interest to keep the rotational speed constant when running the tests, and acquiring the PAT characteristics, an optical sensor, which counted every passing of this small reflector tape, was introduced. By coupling this to a clock function, this would serve as an adequate rpm-indicator.

In order to obtain and collect the data an Arduino Nano unit was used. An Arduino is an open-source electronics platform, which made it possible to transform the analog measurements into digital output [15]. This is a very cheap and available technology, and such a unit was used to log all of the data from the sensors mentioned above.

As for the generator, the initial idea was to use the pump's induction motor as an asynchronous generator. This solution is far cheaper than acquiring an expensive synchronous generator, especially for sizes up to $30kW$ [4]. In addition to being the most cost efficient option,

(a) (b)

Figure 3.3: a) Insertion of permanent magnets into the rotor - b) stator.

it will also result in an easier installation, as the PAT and generator come as one unit. However, in such a set up there may be problems in achieving excitation. A solution to this is to use an arrangement of capacitors to introduce the required reactive power [4]. Another possibility, introduced by co-supervisor Mdee Ombeni, was an approach in which the generator rotor was equipped with four permanent magnets. Thus modifying the asynchronous induction machine into a synchronous generator. This can be seen in figures 3.3a and 3.3b, which displays the rotor with the permanent magnets, and stator, respectively. At this stage however, the output voltage only reached values of between $5V$ and $7V$, due to various complications. Therefore, in order to fix this, three $100\mu F$ capacitors were used to achieve the expected voltage output of around $240V$.

In the end, due to the problems encountered, too many uncertainties, and limited time, no useful data was attained during the time at UDSM. The last straw, however, was the limitations of the available feed pump and motor. Run at maximum capacity it was only able to deliver about $120m^3/h$. In comparison, it was estimated that the flow had to be around $240m^3/h$ in order to reach the predicted best point of this specific PAT. Thus, no proper conclusions could be drawn of the symmetry method's accuracy. This was a setback for the project, which had to

take a new approach. The new plan included ordering a new pump, and to prepare a new test rig for testing and validation at NTNU.

3.2 Pedrollo FG 32/160B

In order to conduct the tests at the waterpower laboratory at NTNU, a new pump had to be acquired. It was desired that the pump had a size which allowed it to be easily transported to UDSM after the tests, thus the decision fell on the modest sized *Pedrollo FG 32/160B*. The first thing that had to be done was to remove the spiral casing, and manually measure the impeller geometry. The geometry specifications relevant to the symmetry method can be found in table 3.2.

This pump is designed for two rotational speeds, 1450 and 2900 rpm. As mentioned previously, it is far more economical to use a pump's induction motor as a generator when setting up a PAT driven power plant. A criteria for doing so is to operate the PAT at the same rotational speed as the induction motor is designed for. When investigating the symmetry method's validity, running the pump at 2900 rpm required sensors and equipment of a higher range than what was available during the testing period. Therefore, the choice landed on running the pump and PAT at a speed of 1450 rpm. However, the characteristic curves and performance data supplied by the manufacturer were only attainable at 2900 rpm, where the pump is said to have an efficiency of 58%. As the efficiency can expected to be of approximately the same order for both rotational speeds, an assumption was made to assign the same efficiency, 58%, to the *Pedrollo FG 32/160B* at 1450rpm as well. At this best efficiency point, the pump's data sheet indicated a discharge of $Q_p = 9m^3/h$ and a head of $H_p = 5.75m$.

After measuring the pump impeller geometry, the values of table 3.2 were inserted into the symmetry method, producing the predicted PAT characteristic curve. Sharma's prediction method, as seen in equations 2.1 and 2.2, was also applied, with the input $\eta_p = 0.58$.

Table 3.2: Pump impeller geometry and rotational speed of Pedrollo FG 32/160B.

Parameter	Value	Unit
Inlet diameter $D_{1,p}$	51	mm
Outlet diameter $D_{2,p}$	153	mm
Inlet height $B_{1,p}$	30.4	mm
Outlet height $B_{2,p}$	5	mm
Outlet blade angle $\beta_{2,p}$	29	°(degrees)
Rotational speed n	1450	rpm

Figure 3.4: The pump impeller of Pedrollo FG 32/160B.

3.3 Experimental setup NTNU

After acquiring the new pump, the new test rig had to be built. The test rig was modelled in Creo Paramterics 3D Modelling Software, as seen in figure 3.5. It was erected as the illustration shows, and equipped with the necessary instrumentation. During testing the pump was run both as a pump and in turbine mode as a PAT, hence, the flow direction differed. In turbine operation the water came down from the top of the figure into a 600mm diameter pipe. From here the cross-section of the piping decreases to a diameter of 200mm where the valve was

located. After the valve, the diameter was further coned down to $50mm$, where the flow faced a bend. Further, the water was transported rightwards in the figure, passing through the flow sensor, before the cross-section once again was reduced to a diameter of $32mm$, which matched the inlet of the PAT. Then, the water passed through the impeller, before leaving the PAT through a $50mm$ diameter pipe into the reservoir.

In pump operation, the flow direction, and the path of the water, was opposite. The water was pumped up from the bottom reservoir and out through the top of the illustrated piping. From here the water was transported along a piping system not showed in the figure, before it was returned down into the reservoir.

The laboratory, where the tests were conducted, was equipped with a pressure tank, which supplied water for PAT testing. For pump operation testing, the bottom reservoir was used. In both modes the flow rate was controlled manually by using the valve. The flow rate was then measured with the *Optiflux 2000 C* flow sensor. In order to establish corresponding pressure head values to each flow measurement, the inlet and outlet pressures had to be logged at the positions labelled as $P1$ and $P2$ in figure 3.5. The two pressure sensors consisted of one *GE UNIK 5000* with a range of $0-5bar$ gage, and one *GE Druck PTX 1400* designed for a gage pressure $0-4bar$.

To be able to calculate the efficiency of the PAT and pump, the torque was measured with a *HBM T22/200Nm* sensor, which was mounted with flexible couplings on the shaft between the pump and the motor. Also, an rpm-sensor was mounted at the same location. This sensor was a similar solution to what was used at UDSM, in which an optical sensor counted every passing of a small reflector tape on the shaft. All the sensor data were monitored and logged in a specially designed LabVIEW program, attached in appendix C.

To the right of the pump, a $3kW$ *Lönne* electric motor was positioned. This was further coupled to a frequency converter, which made it possible to keep the rotational speed close to constant throughout the testing.

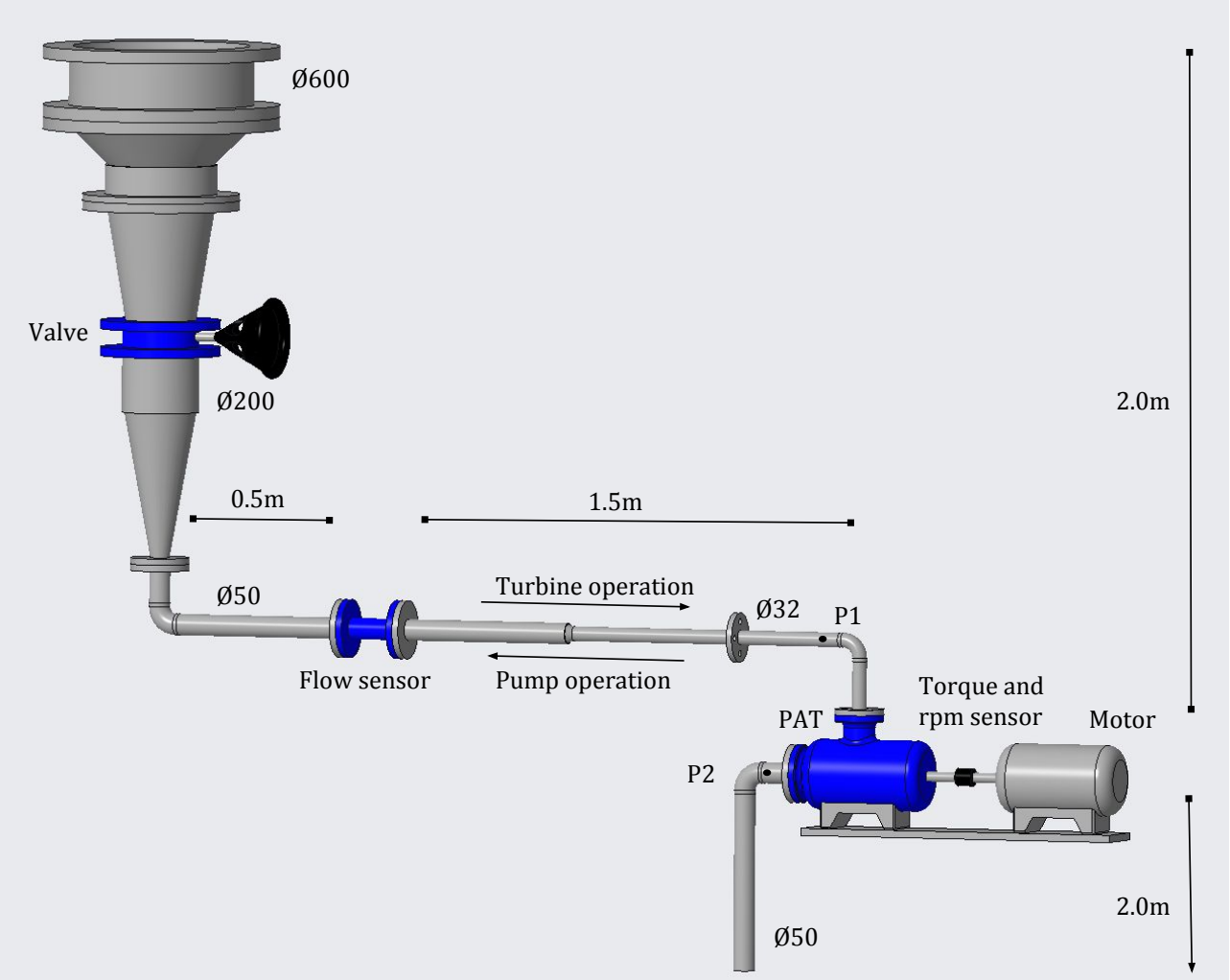

Figure 3.5: Illustration of test rig constructed at NTNU, designed in Creo.

3.4 Data acquisition

3.4.1 Pump operation

When testing the pump, and obtaining its $H-Q$ characteristics, the amount of water pumped up was controlled by turning the valve, located to the left in figure 3.5. By controlling the volume flow, the corresponding head values could be calculated for different opening degrees.

As previously stated, the symmetry method's input is the pump geometry, rotational speed and an assumption of the inlet meridional velocity. In the development of the prediction method, and in the paper prepared for the conference at Kathmandu University (appendix A), the as-

sumed inlet meridional velocity was based on numbers given by Bye (1967)[12]. For a modest sized pump like the *Pedrollo FG 32/160B*, $c_{m1,p}$ was set a value of $2.5 m/s$. During testing however, it became clear that this assumption was way to large for a pump with flow rates of this magnitude. Therefore, the assumption of $c_{m1,p}$ needed to be modified. The alternative solution was to use mass conservation of the flow to estimate a more appropriate velocity component, based on the flow at the pump's BEP. As the inlet and outlet geometry was known, $c_{m1,p}$ could be directly calculated as:

$$c_{m1,p} = \frac{Q_p}{\pi B_1 D_1} \tag{3.1}$$

By using the equation above, and inserting the geometry parameters from table 3.2 as well as the rated flow given by the manufacturer, the meridional velocity component came out to be $c_{m1,p} = 0.513 m/s$.

Another problem that arose during testing was complications with the torque sensor. The output signal from the sensor was extremely unstable, and not anywhere close to expected torque values. Based on previous experience in the laboratory, one possible reason for this was said to be the frequency converter, which has a tendency to disturb the sensor signals. By not being able to correctly measure the torque, and consequently the power, the efficiency and BEP would be hard to find. Due to time limitations, a proper solution of making the torque sensor work was not found. However, the frequency converter had an option of measuring the power, which in turn was used to calculate the efficiency. It should be stressed that this efficiency is not an entirely correct representation, as it contains the losses in both the motor/generator and the frequency converter itself. Still, as the main intention was to find head and flow values at BEP, and not necessarily accurate efficiency values, this solution would serve as a respectable indication.

3.4.2 Pump as Turbine

During PAT testing, and similar to the testing in pump mode, the water flow was controlled by adjusting the valve. The water was supplied from a pressure tank in the laboratory, which have an available head of approximately $20m$. It was important to achieve a pressure head of this magnitude, as the PAT was not operative at $1450rpm$ for lower pressures. Similar to testing in pump operation, the efficiency values were calculated based on the power measured by the frequency converter.

3.5 Calibration and uncertainty

Before the tests could be performed, the appropriate sensors had to be calibrated. This calibration comes with an uncertainty. All measurements done during the tests also have uncertainties due to inaccuracies in the instruments and random variations of the measured property. Because of this, it is always necessary to conduct an uncertainty analysis. A thorough description of the calibration, and the uncertainty analysis, can be found in appendix B, along with the calibration certificates. The results from this analysis is summarized in table 3.3 below.

As already stated, due to complications with the torque sensor, the efficiency was not found the conventional way. It was instead found through the power calculated by the frequency converter, which will contain losses from both the motor/generator and the converter itself. Thus, there are major uncertainties associated with the efficiency value η. However, as the value of the efficiency is not the main concern, but rather the location of the best efficiency point, this value will still be useful. To account for the uncertainty in the location of the BEP, an error was assumed in the manual reading from the display on the frequency converter. The power magnitude was varying considerably, hence a rather large uncertainty of $\pm 5\%$ was assumed.

Table 3.3: Total uncertainty for the experiment parameters.

Quantity	Calibration Uncertainty	Mean Measured Uncertainty	Total Mean Uncertainty
P_1	±0.495%	±3.855%	±3.886%
P_2	±1.154%	±3.182%	±3.384%
Q	±0.231%	±0.003%	±0.231%
H	–	±0.462%	±0.462%
η	–	–	±5%

As table 3.3 reveals, the uncertainty was also high in the two pressure sensors. It was observed that the signals were quite unstable during testing, and the uncertainty depicts the random errors from the high degree of variation in the system.

CHAPTER 4

Results

As the initial tests at UDSM in Tanzania did not produce any valuable outcome, the only appropriate results are from the tests done at NTNU. Thus, the following results, which will be discussed and used to investigate the symmetry method's validity, is solely from the tests conducted there.

4.1 Pump testing

By testing the *Pedrollo FG 32/160B* in pump operation, its $H-Q$ characteristic was produced. This can be seen in figure 4.1. Also seen in figure 4.1, is the pump's efficiency curve with respect to flow. It can be observed that both curves are similar in shape to what was expected from figure 2.2. By studying the power computed by the frequency converter, a rough estimate of the maximum pump efficiency could be calculated. The estimate came out to be $\eta_p = 0.45$. This in turn supplied the head and flow values at the predicted BEP, $H = 5.91m$ and $Q = 8.95m^3/s$ respectively. Compared to the pump efficiency of $\eta_p = 0.58$ given by the manufacturer, the efficiency calculated from the frequency converter is far off. However, the BEP values of head and flow are strikingly similar, as seen in table 4.1. The estimated value of head deviates 2.7%, while

flow deviates by 0.6%, compared to the experimental values. This shows that even though the efficiency is lower due to the various losses, it still serves as a good indication of where the BEP lies.

Using the rated volume flow found through testing, and applying equation 3.1, the actual $c_{m1,p}$ at BEP was calculated. This can be seen in comparison with the previously estimated $c_{m1,p}$-value, based on the rated values in the pump's data sheet. The latter of which was used as input to the symmetry prediction method. Both meridional velocities are also presented in table 4.1, where the estimated value deviates 0.4% from the test value.

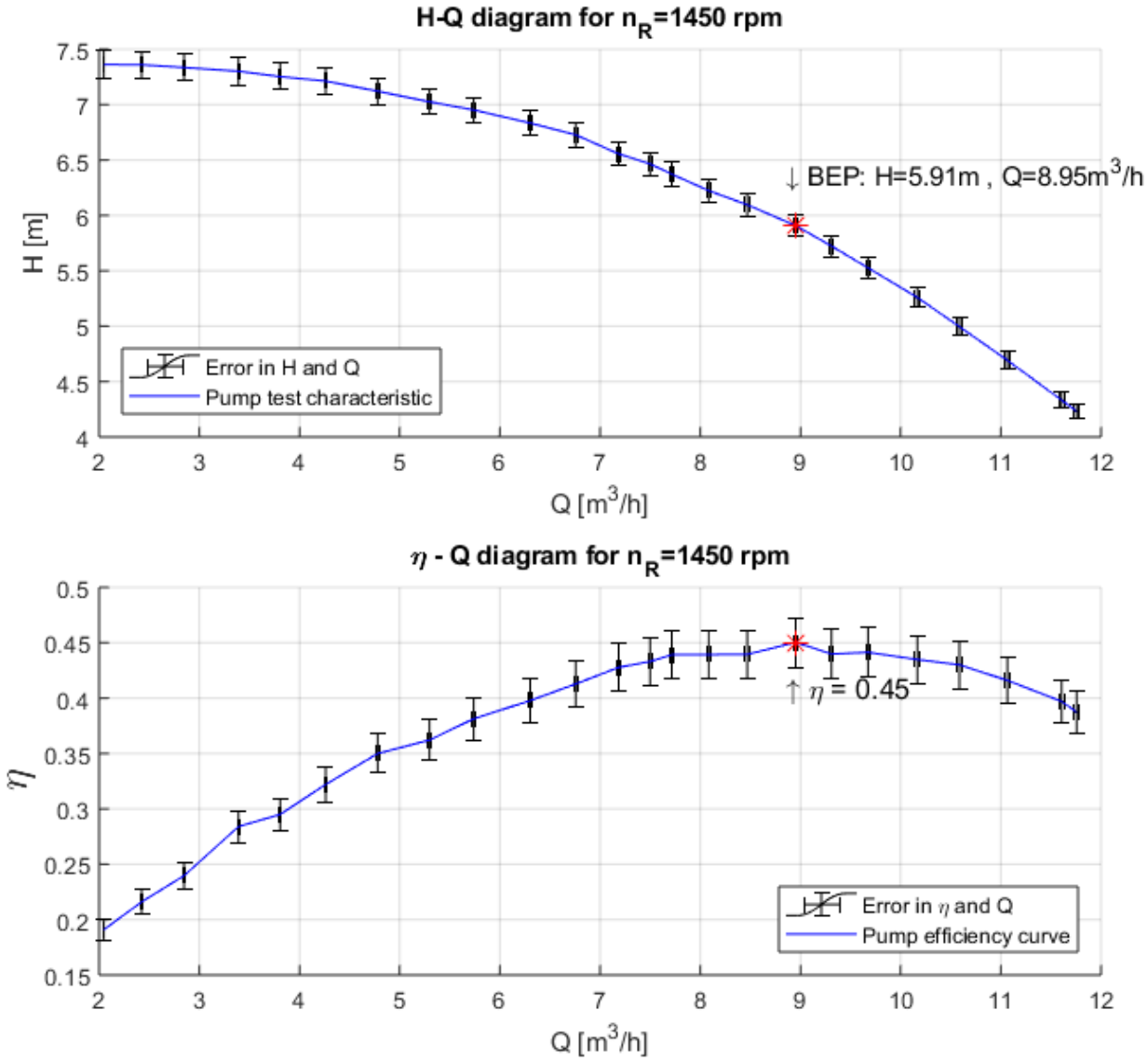

Figure 4.1: $H-Q$ characteristic and efficiency curve from pump testing.

Table 4.1: Comparison of test and estimated values in pump operation.

Parameter	Test value	Estimated (given) value	Unit
Rated head H_p	5.91	5.75	m
Rated flow Q_p	8.95	9	m^3/h
Inlet meridional velocity $c_{m1,p}$	0.511	0.513	m/s
Pump maximum efficiency η_p	0.45	0.58	–

4.2 PAT testing

Similar to the pump testing procedure, the PAT's $H-Q$ characteristic was established through adjusting the valve and incoming flow. This characteristic can be seen in figure 4.2, which also follows the typical performance curve from 2.2. Moreover, in the same plot, the symmetry method's prediction is presented along with its predicted best efficiency point, marked with a red asterisk. Additionally, the pump efficiency found in the data sheet of *Pedrollo FG 32/160B* was inserted into Sharma's prediction method equations (2.1 and 2.2), which produce a BEP as marked by the pink asterisk. It is clear that the characteristic predicted by the symmetry method is off-target, compared to the actual characteristic attained from the tests. Thus, investigation of how to improve the method's precision is required.

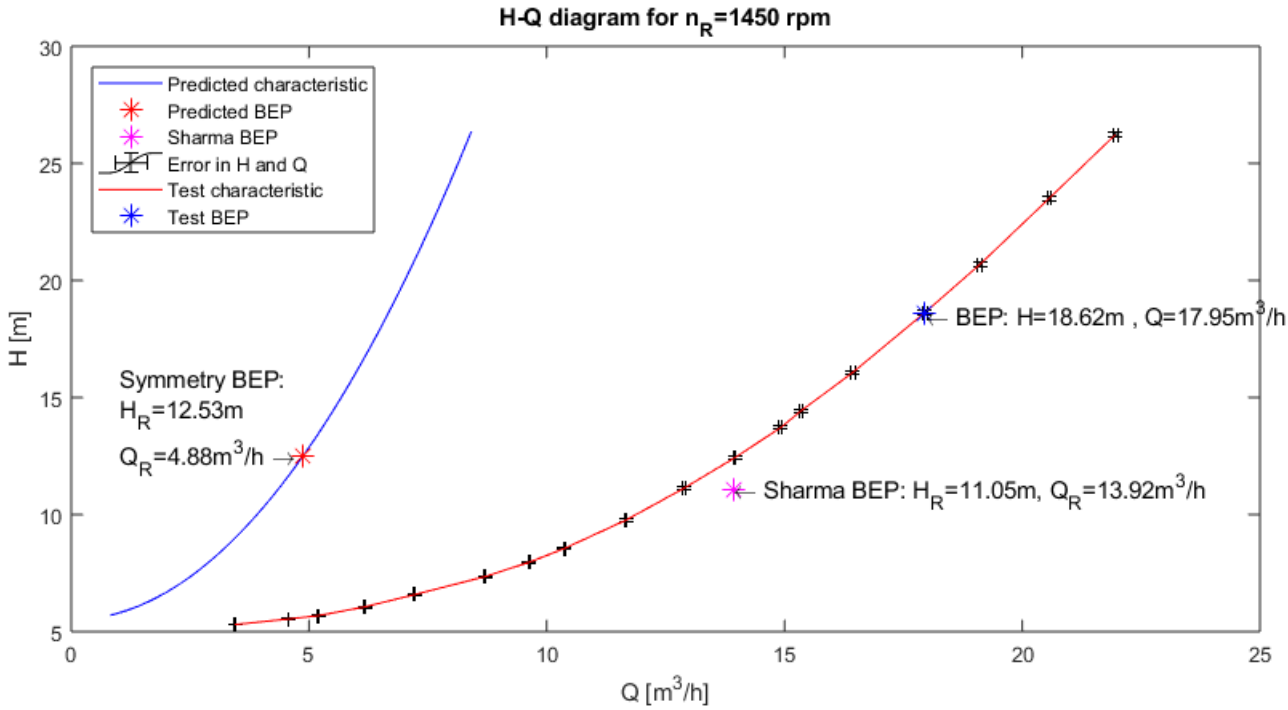

Figure 4.2: $H-Q$ characteristics, both predicted and acquired through testing.

Figure 4.3 presents the efficiency calculated in PAT operation. The maximum efficiency is estimated to be at $\eta_t = 0.395$, which provides the BEP values of head and flow in figure 4.2. It is important to note the uncertainty of the efficiency in figure 4.3, and that the location of the best efficiency point in figure 4.2 could change in line with this uncertainty. It can also be observed that the maximum efficiency of the PAT is below that of the pump. However, the value must not be taken too literally, as the method of calculating the efficiency is subjected to considerable losses. This was expressed in the previous section, where the pump maximum efficiency estimated with this method, being 45%, and the efficiency given by the manufacturer, 58%, gave practically the same head and flow values.

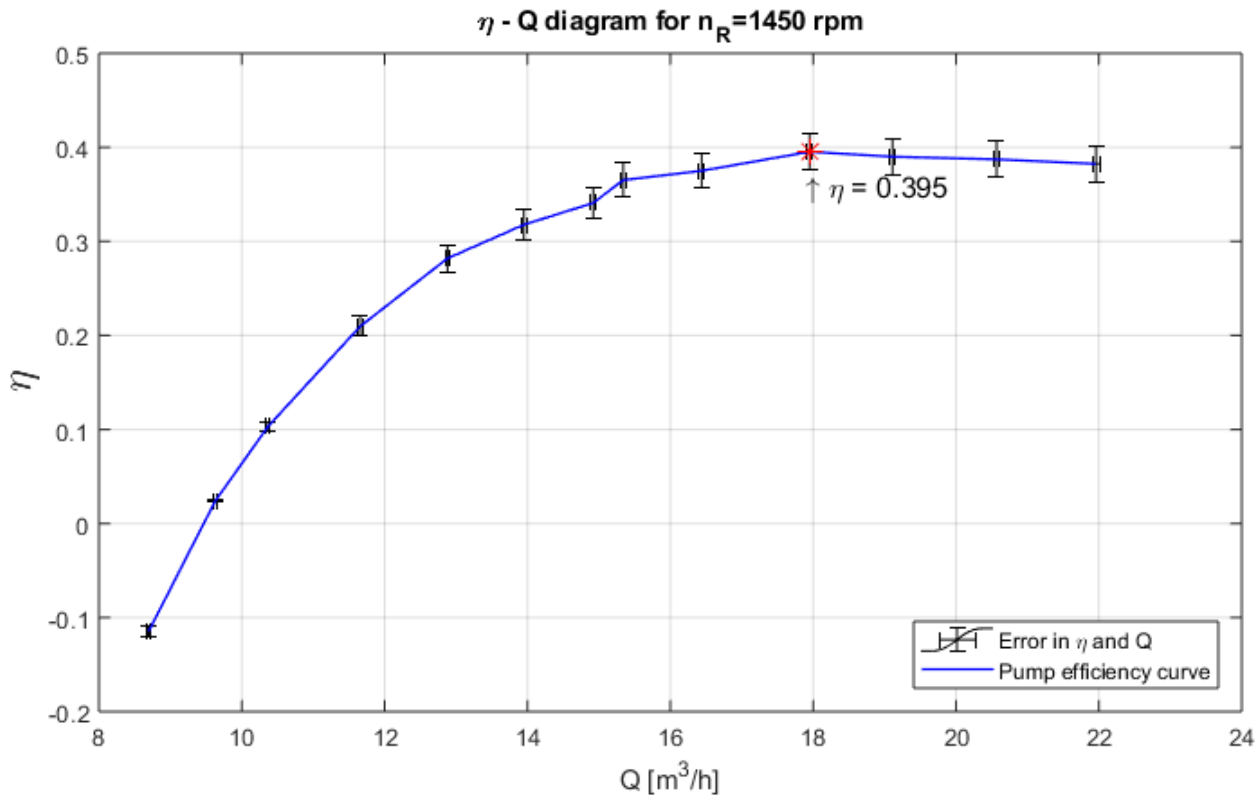

Figure 4.3: Pump as turbine efficiency curve.

4.2.1 Velocity diagrams

Based on the measured best efficiency flow in both pump and turbine operation, impeller geometry and operating conditions, the velocity diagrams could be constructed. The upper portion of figure 4.4 shows the velocity diagram of the pump outlet, and the PAT inlet. Similarly, the lower portion displays the pump inlet and PAT outlet. It can be observed that the diagrams are not strictly symmetrical, as assumed in the symmetry method, and do not look exactly like the diagrams in figure 2.4. The turbine meridional velocities are significantly larger than those in pump mode. As $c_{m1,t}$ is larger than $c_{m2,p}$, angle $\alpha_{1,t}$ is also larger than $\alpha_{2,p}$, which makes the mirroring of α not entirely acceptable. This is something that has to be accounted for in order to improve the accuracy of the symmetry method.

Likewise, as the flow and meridional component is larger in turbine mode, $c_{m2,t}$ is also greater than its pump counterpart. This is illustrated in the lower part of figure 4.4. Moreover, the common assumption of no swirl at the pump inlet and turbine outlet is still enforced, which

eliminates any c_u-components in this diagram. In reality, one might expect some rotation at the PAT outlet, which in turn would give the flow a relative flow angle $\beta'_{2,t}$, and introduce a tangential component of the absolute velocity. An estimate of $c_{u2,t}$ can be made by the use of Euler's equation 2.4, if a good measure of the hydraulic efficiency is known.

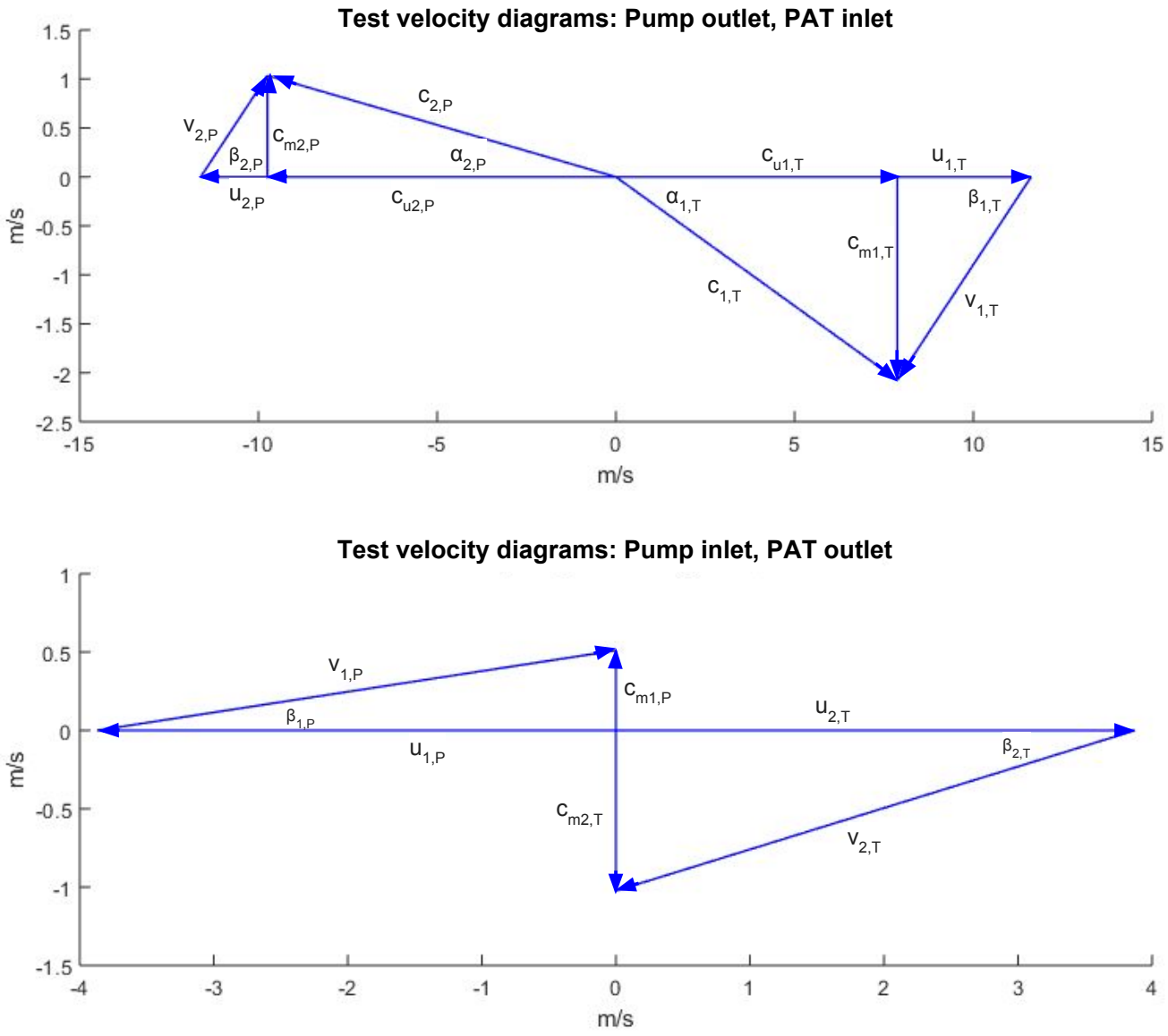

Figure 4.4: Velocity diagrams from test results.

4.3 Potential improvements

By looking at figure 4.4, and paying attention to the axes, it becomes clear the meridional velocities do not follow the initial assumption of $c_{m2,p} = 1.1c_{m1,p}$. One way to modify this assumption is to utilize the fact that the flow rate is unchanged through the impeller. In that way the relationship between $c_{m1,p}$ and $c_{m2,p}$ is only dependent on the inlet and outlet geometry.

$$\frac{c_{m2,p}}{c_{m1,p}} = \frac{\frac{Q_p}{A_{2,p}}}{\frac{Q_p}{A_{1,p}}} = \frac{A_{1,p}}{A_{2,p}} = \frac{\pi B_{1,p} D_{1,p}}{\pi B_{2,p} D_{2,p}} = \frac{B_{1,p} D_{1,p}}{B_{2,p} D_{2,p}} \tag{4.1}$$

For this specific pump, the relationship turned out to be as in equation 4.2. By implication, and through the assumptions of the symmetry method, the meridional components in turbine mode has the inverse relationship.

$$\frac{c_{m2,p}}{c_{m1,p}} = \frac{c_{m1,t}}{c_{m2,t}} = 2.03 \tag{4.2}$$

If the new relationship in equation 4.1 is applied to the symmetry method, the predicted characteristic moves closer towards the $H-Q$ curve from the experiments, as represented by the dashed line in figure 4.5.

After this alteration it was also observed that the $c_{m,t}$-components from the tests were greater than the $c_{m,p}$-components from the pump tests. To account for this, the prediction of $c_{m1,t}$ is modified accordingly:

$$c_{m1,t} = k c_{m2,p} \tag{4.3}$$

The constant k is an empirical value which accounts for the asymmetry from pump to turbine operation. From this single PAT test, the value of the constant was found to be $k = 2.005$. The predicted PAT characteristic with this additional improvement is shown in figure 4.5, represented by the solid blue line. It is seen that the flow predicted is a lot closer to the actual best efficiency point than what was found earlier. On the other hand, the pressure head is still a ways from the test BEP. This will be subjected to discussion later on.

A summary of the significant parameters are presented in table 4.2. It contains values from the symmetry method, the real test values, as well as the new and improved values after the

second modification.

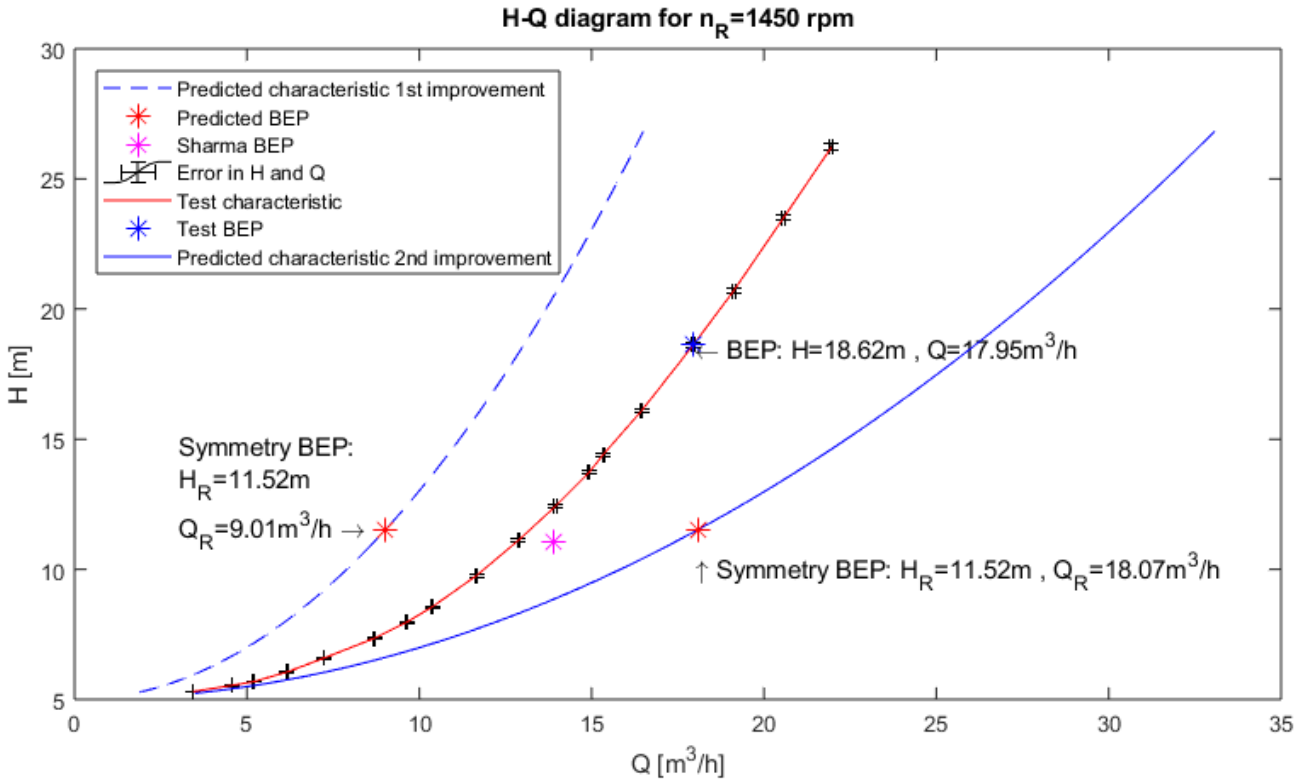

Figure 4.5: $H-Q$ characteristics, improved predicted curves and the one acquired through testing.

Table 4.2: Comparison of PAT parameters - tests and predictions.

Parameter	Symmetry method prediction	Improved symmetry method	Test value
$c_{m1,t}$	$0.565 m/s$	$2.089 m/s$	$2.075 m/s$
$c_{m2,t}$	$0.513 m/s$	$0.513 m/s$	$1.024 m/s$
$\alpha_{2,p}$	3.05°	6.11°	6.06°
$\alpha_{1,t}$	3.05°	12.11°	14.76°
$H_{R,t}$	$12.53 m$	$11.52 m$	$18.62 m$
$Q_{R,t}$	$4.88 m^3/h$	$18.07 m^3/h$	$17.95 m^3/h$

CHAPTER 5

Discussion

As already explained, the initial tests at UDSM did not produce any valuable results. However, the tests granted us a beneficial understanding on how to plan the experiments that were conducted at NTNU later on. Also, the visit proved to be a useful experience in order to understand the conditions and limitations of doing scientific research in developing countries. Additionally, the stay confirmed what has been suggested previously, that PATs can be a favorable technology in areas where proper equipment and competence is scarce, and simpler and more robust solutions are a necessity.

5.1 Pump testing

Even though the main goal of the testing was to verify how well the symmetry method predicted the actual PAT characteristic, the *Pedrollo FG 32/160B* was first tested as a pump. This was done in order to investigate if the real best efficiency point of the pump was the same as the one given by the manufacturer, and to evaluate the $c_{m1,p}$-assumption. What was found was that the two best efficiency points were very much in accordance with each other. However, the location of the BEP may of course vary in accordance with the uncertainty, but it is still within an acceptable

range.

Initially, as an input to the symmetry method, $c_{m1,p}$ was assumed based on suggested values given by Bye (1967)[12]. However, during the pump tests it was observed that the assumed value was way to large, and had to be modified. As already mentioned, the new approach was then to use equation 3.1 to calculate $c_{m1,p}$ based on the pump's rated flow. As the test results were so similar to what was stated as the pump's BEP in the data sheet, the real $c_{m1,p}$ that was calculated only differed about 0.4% from the one calculated in advance, and applied in the prediction. This can be seen in table 4.1. Also seen in the table is that this modification influenced the α-angles, and pushed the predicted values closer to the real test values. Therefore, in this case, it can be justified to use the information from the pump manufacturer as input to the model.

Despite acquiring very similar BEP values, the calculated efficiency from the tests did not match the pump's rated efficiency. This was most likely because the efficiency was found through the frequency converter, and not by the conventional approach of measuring the shaft torque. As stated previously, measuring the power through the frequency converter contain the losses from both the motor/generator and the converter itself, and is therefore not an entirely legitimate representation. Still, as the BEP values turned out to be as similar as they were, it indicates that the location of the maximum efficiency found was comparable.

5.2 PAT testing

After the pump tests, where the approach for finding $c_{m1,p}$ was revised, the characteristic in figure 4.2 was predicted. Also in the same plot, the characteristics from the experimental data is presented, along with Sharma's best efficiency prediction. It is clear that the symmetry method predicts a curve, and a BEP, which is far below what was found during testing, and what Sharma predicts. This is especially seen in the amount of volume flow. The point of highest efficiency was determined by the relationship in figure 4.3, and came out to be 39.5% at a flow of $17.95 m^3/s$. In the region around this point, the efficiency varies little with respect to flow. Therefore, a tiny shift in efficiency will result in a large shift in the flow, and consequently the location of the PAT's best efficiency point. This is especially important to note, considering the questionable way the power was logged, and found, through the frequency converter.

It may also be observed that the best efficiency point predicted by the symmetry method has a lower flow than the pump's BEP, presented in figure 4.1. This is not in agreement with what has been found by previous studies on pumps as turbines, where the PAT BEP is expected to be higher in both head and flow, than the BEP in pump operation [6].

As the experimental BEP had a flow of more than three times the one predicted by the symmetry method, it was evident that some modifications had to be done. By investigating the velocity diagrams in figure 4.4, it is obvious why the predicted flow is of the magnitude that it is. Whereas the predicted curve is based on absolute symmetry between pump and turbine operation, the velocity diagrams from the tests indicate a clear asymmetrical relationship. One possible explanation for this relationship, could be because of the gap in head between pump and turbine operation, seen in figure 2.3. The gap indicates that the transition between pump and turbine mode is not necessarily straight forward, and that the symmetry assumption might be a little weak. Thus, the goal became to find possible improvements which could strengthen the model.

5.2.1 First modification

One of the assumptions done in the early stages of the development of the model, was that the pump would accelerate the meridional velocity component by 10%. The velocity diagrams in figure 4.4 reveal that the acceleration is significantly higher. Thus, the modification presented in equation 4.1 was applied. This new way of determining the $c_{m,p}$-ratio is in line with the symmetry method's approach, namely to use impeller geometry data as the only input. The dashed line in figure 4.5 represents the new predicted characteristic, with this modification applied. It can be observed that the BEP flow is almost double to what it was before, but still only half of what the tests indicate. At this point, the predicted BEP in turbine operation increases past the BEP flow in pump operation, making the symmetry prediction model more analogous to what has been found in previous studies. Still, this modification does not address the asymmetry in the velocity diagrams. Hence, an additional modification was needed in order to account for this.

5.2.2 Second modification

When studying figure 4.4, one can see that the reason for the asymmetry in the velocity diagrams is the results of a much larger meridional velocity component in turbine BEP operation, compared to pump operation. The reason could be because of the previous mentioned gap in figure 2.3. Consequently, it is not entirely correct to directly mirror $c_{m2,p} = c_{m1,t}$ and $c_{m1,p} = c_{m2,t}$. In fact, the $c_{m,t}$-components turned out to be about two times larger than the $c_{m,p}$-components. To deal with this, the empirical relationship in equation 4.3 was enforced.

From this single PAT test, the value of the constant was found to be $k = 2.005$. However, establishing a general empirical factor based on one test alone, is dubious at best. Consequently, more PATs must be tested in order to conclude on a more universal constant k.

Introducing an empirical relationship like this defines a turning point the in development of the symmetry model. By moving away from the symmetry assumption, the model's name loses credibility, and it takes a step towards the many already existing prediction methods presented earlier. Still, the only input to the model remains the impeller geometry, but the value of the constant k will need to be refined through further testing.

The most recent predicted characteristic, with the first and second modifications combined, result in the solid blue line in figure 4.5. One can see that the latest modification accounts for the difference in flow, and the newly predicted BEP is very similar in volume flow to the test BEP. On the other hand, the predicted pressure head has remained the same value throughout, and is about seven meters below the test's best efficiency point.

At this stage it is of interest to draw a comparison between the symmetry model, and Sharma's prediction model. Sharma's model, which Williams (1994) [1] considered to be the most accurate existing model at the time, also predicts a head of the same range - far below what was found during testing. Sharma's predicted BEP is expressed by the pink asterisk in figure 4.5.

5.2.3 Assumptions and inaccuracies

One possible explanation of why Sharma's and the symmetry prediction models fall short in evaluating the BEP head, might be because of uncertainty in the location of the BEP itself. As already mentioned, the highest efficiency was found in a region with little variation with respect

to flow. Because of this, a small variation in efficiency, will result in a significantly larger change in flow. This change in flow will in turn result in an even larger shift in the BEP head. The reason for this is the steepness of the test characteristic curve in figure 4.5. In short, an inaccurate measure of the efficiency will have a great impact on the rated head. Because of the large assumed uncertainty in η, seen in figure 4.3, the flow could range from about $16.5 - 21 m^3/h$. If the lower limit is the case, the location of the experimental best efficiency point in figure 4.5 could move all the way down to a head of approximately $15m$. Thus, the experimentally measured head at BEP moves closer towards what has been predicted by both Sharma, and the symmetry method.

Another factor that could impact the head prediction is one of the assumptions in the symmetry method. As described in section 2.4.1, a swirl free flow is assumed at the inlet of the pump, and outlet of a turbine. If rotation at the turbine outlet is included, equation 2.4 gets a $c_{u2,t}$-component, which could alter the prediction of H_R. As mentioned previously, an estimate of $c_{u2,t}$ can be made by the use of Euler's equation 2.4, if a good measure of the hydraulic efficiency is known.

A separate aspect that hasn't been addressed is the effect of friction and shock losses. In turbine mode, these losses will contribute to a reduction of the net head. Therefore, it might be expected that the actual best efficiency point in PAT mode lies even higher than what has been predicted, to account for these losses. Further, when applying symmetry, a decision was made not to include the slip from pump operation. Slip would have altered the blade angle to the relative flow angle, and consequently changed the velocity diagram in turbine mode. This can be justified as the effect of slip in turbine operation, compared to pump operation, will be modest, and therefore may be neglected [3].

Finally, the hydraulic efficiency was for simplicity set to 1, even though the pump was measured to have a maximum efficiency of $\eta_p = 0.45$. By including a more trustworthy hydraulic efficiency into Euler's pump and turbine equations (2.3 and 2.4), the predicted head in turbine mode would increase, and the accuracy of the prediction model could be enhanced.

5.2.4 Additional challenges and further work

As seen from the results, the PAT's maximum efficiency was measured to be of approximately the same order as the pump's efficiency. Even though the actual value of the efficiency measurement may be questioned, it is fair to say that the PAT's efficiency will not exceed the efficiency supplied by the pump manufacturer. Therefore, as a pump's efficiency is significantly lower than a custom made turbine, one will have to consider if it is profitable to invest in a PAT-driven power plant. However, as stated earlier, this is mainly a solution appropriate for developing countries and rural areas, where low investment costs are far more important than efficiency.

On a separate note, a drawback to the symmetry prediction method presented, is that the impeller geometry has to be manually measured. By having to remove the spiral casing of the pump, the usage of the model is not exactly straight forward. This will usually require actually purchasing the pump, as pump manufacturers seldom publish this information. Hence, the goal of being able to pick a suitable pump right off the shelf, which correlates to a site's given conditions, is not satisfied. For that reason, the selection process is optimal only if pump manufacturers make such data available. Another idea is for pump manufacturers to apply such a prediction method to their own pumps, and publishing predicted PAT characteristics to potential buyers, instead of having to test the pumps themselves.

Potential further development of the symmetry method may include obtaining a more general constant k, found in equation 4.3. As for now, the constant's value is based on one single PAT test, but by testing several pumps as turbines, the credibility of which will be strengthened. In that way, different k values for different sizes and types of pumps may be established. Further, if a way is found to quantify the different losses in PAT operation, a better prediction should be achievable. Lastly, if future tests are carried out with an operational torque transducer, a better estimation of the uncertainty of η could be made. Also, the location of the best efficiency point could become more accurate.

CHAPTER 6

Conclusion

The objective of this thesis was to investigate the validity of the already developed symmetry method, which is based solely on the pump's impeller geometry. For this reason, experimental tests were conducted in the laboratory to study the PAT's $H-Q$ characteristic. The tests revealed that some of the assumptions in the model were inadequate, and had to be adjusted and improved accordingly.

In order to analyze the model, and its assumptions, the pump was tested in both pump and turbine operation. The results from these tests made it clear that the assumption of total symmetry in the velocity diagrams between pump and turbine operation, was not completely valid. Therefore, to account for this, two potential improvements were proposed. These improvements enhanced the prediction model in the way that the predicted PAT characteristic moved closer towards to the experimentally produced characteristic. However, in order to strengthen the new improvements, and to make the prediction model more general, additional tests must be carried out. This is especially important with respect to finding a more general empirical constant k, as the result from one single PAT test is uncertain at best.

It is also uplifting that the predicted characteristic is in line with already established prediction techniques, and produce a quite similar best efficiency point. However, because of the lack

of guide vanes, it is difficult to operate a pump as turbine at its BEP. Therefore, it can truly be advantageous that the symmetry method produces a full characteristic, to be able to foresee the PAT's performance at either side of this point.

One drawback with the method is the fact that the impeller geometry has to be measured manually. This will often include purchasing and dismantling the pump. Hence, the model will be significantly easier to use if pump manufacturers begin to make such geometry information public. In that case, and if further refinement of the constant k is done, the proposed prediction method could become both accurate and simple to use. Also, even though the efficiency of a PAT is low compared to specifically designed hydro turbines, it is still a highly relevant option. This is especially profitable in developing countries and rural areas, as these areas will benefit greatly from an accurate prediction model, in order to maximize the power output available.

Bibliography

[1] A. Williams. The turbine performance of centrifugal pumps: a comparison of prediction methods. *Proceedings of the Institution of Mechanical Engineers, Part A: Journal of Power and Energy*, 208(1):59–66, 1994.

[2] S. V. Jain R. N. Patel. Investigations on pump running in turbine mode: A review of the state-of-the-art. *Renewable and Sustainable Energy Reviews*, 30:841–868, 2014.

[3] J. M. Chapallaz P. Eichenberger G. Fischer. *Manual on pumps used as turbines*. Vieweg, 1992.

[4] A. Williams. Pumps as turbines for low cost micro hydro power. *Renewable Energy*, 9(1-4): 1227–1234, 1996.

[5] S. Derakhshan A. Nourbakhsh. Experimental study of characteristic curves of centrifugal pumps working as turbines in different specific speeds. *Experimental thermal and fluid science*, 32(3):800–807, 2008.

[6] J. Fernandez E. Blanco J. Parrondo M. T. Stickland T. J. Scanlon. Performance of a centrifugal pump running in inverse mode. *Proceedings of the Institution of Mechanical Engineers, Part A: Journal of Power and Energy*, 218(4):265–271, 2004.

[7] P. N. Garey. Using pumps as hydro-turbines. *Hydro Review*, pages 52–61, 1990.

[8] A. Kjølle. Mechanical equipment. *Waterpower laboratory, NTNU*, 2001.

[9] A. Williams. *Pumps as turbines: a user's guide.* Intermediate Technology, 1995.

[10] B. H. Teuteberg. *Design of a pump-as-turbine microhydro system for an abalone farm.* PhD thesis, Stellenbosch: University of Stellenbosch, 2010.

[11] H. Brekke. Pumper & turbiner. *Vannkraftlaboratoriet NTNU*, 2003.

[12] G. Bye. *Pumper.* Universitetsforlaget, 1967.

[13] T. K. Nielsen. Simulation model for francis and reversible pump turbines. *International Journal of Fluid Machinery and Systems*, 8(3):169–182, 2015.

[14] International Electrotechnical Commission. *IEC 62097: Hydraulic machines, radial and axial - Performance conversion method from model to prototype.* 2009.

[15] M. Margolis. *Arduino Cookbook: Recipes to Begin, Expand, and Enhance Your Projects.* " O'Reilly Media, Inc.", 2011.

[16] International Electrotechnical Commission. IEC 60193: Hydraulic turbines, storage pumps and pump-turbines - model acceptance tests. 1999.

[17] B. W. Solemslie. Compendium in instrumentation, calibration uncertainty analysis. 2010.

[18] P. T. Storli. Modelltest av francis turbin, 2006.

APPENDIX A

Paper written for CRHTVIII'18

The following section contains a research paper written for the 8th edition of the annual *Symposium on Current Research in Hydraulic Turbines (CRHTVIII'18)*. The results presented were obtained during the previous project work, where the symmetry prediction method was established. As the derived method, and the theoretical concepts, are quintessential for this thesis, it was considered necessary to present them once more. Therefore, some sections of the following paper may be very similar the thesis you have just read.

Symmetry prediction method for pump as turbine characteristics

Øyvind Albert*, Sondre Skjoldli*, Torbjørn K. Nielsen
Department of Energy and Process Engineering, Norwegian University of Science and Technology, Trondheim, Norway
*Corresponding authors (oyvinalb@stud.ntnu.no, sondsk@stud.ntnu.no)

Abstract. As a cheap and available source of renewable energy, regular centrifugal pumps may be run in reverse to act as hydro turbines. Pumps as turbines (PAT) are especially relevant for isolated rural areas, or in developing countries, where efficiency is not necessarily the highest priority. The main challenge, however, is to be able to pick a suitable pump for a given site, which coincides with the available head and discharge. In order to make this decision, one has to be able to predict how a certain pump will perform in turbine mode. A lot of work has been done in the past to establish such prediction methods, based on tests and empirical correlations. However, the inaccuracies of these methods motivate a new approach, where the performance in turbine mode is based solely on the pump's geometry.

By assuming symmetry at the outlet of a pump to the inlet of a turbine, a method for establishing a PAT' s characteristics, such as $Q_{ed} - n_{ed}$ and $H - Q$ curves, was made. To generalize the method, it was applied to both high and low head pumps. These characteristics were then compared to fictional Francis runners, designed for the same best efficiency point (BEP) values of head and flow. Further, the method was applied to one specific pump, which is scheduled to be subjected to physical tests. Analogous to literature, it was predicted that the BEP operating values of this PAT lies above its original BEP values in pump mode. From these rated BEP values, corresponding PAT characteristics were predicted. Finally, to be able to verify and validate the prediction model, thorough tests are scheduled to be carried out.

1. Introduction

In a time where renewable power production is becoming increasingly important, the motivation to reduce the costs as far as possible also gets a lot of attention. One appropriate technology is to use a pump as a turbine (PAT). By using a regular centrifugal pump, and running it in reverse, one will be able to extract energy from a fluid instead of putting energy into it. The idea is not at all new, but could prove to be increasingly relevant and important for developing countries, and isolated rural areas, where the electricity demand is ever growing [1].

Even though operational and running costs of a hydropower plant are low and affordable, the high initial capital cost in the development of such a plant can truly be a barrier [2]. Additionally, as large-scale generation is not always feasible, there is an increasing interest in small-scale hydropower plants. In these small-scale plants, it can often be hard to justify the construction costs in comparison to the total power generation possible [3]. It is in these situations a PAT can show its full potential, and can prove to be a very suitable technology, because of its low price. The price per kW produced by small-scale hydro power plants, are usually higher than that of large hydro power plants [1]. Therefore, installment of a PAT could be essential in reducing

these costs.

The main obstacle when planning a PAT driven power plant is the difficulty of predicting the optimal turbine characteristics [2]. The primary challenge therefore lies in being able to pick a suitable pump for a given site, which coincides with the available head and discharge. In order to make this decision, one has to be able to predict how a certain pump will perform in turbine mode.

2. Theoretical background

If a centrifugal pump is to be used as a PAT, the advantages and disadvantages has to be carefully weighed up against each other. Firstly, when looking at it from an economic point of view, PATs have a clear advantage. Centrifugal pumps are mass produced all over the world, and are manufactured for a wide range of heads and flows. By being able to pick a centrifugal pump right off the shelf, a PAT will be a significantly cheaper option than a turbine designed for specific conditions. In other words, they are more cost efficient as well as more accessible. What's more is that they are easy to install, easy to maintain, and that spare parts are easily available [2]. As pumps are a more widespread technology than turbines, qualified personnel to conduct repairs and maintenance is also more available.

There are several disadvantages however, besides the aforementioned challenge of predicting the PAT performance. Even though Fernandez et al. (2004)[3] state that the efficiency of a pump running in reverse has almost the same efficiency as in pump mode, it will most certainly not perform as well as a custom made turbine. It may seem as if the pump industry is not as concerned as the turbine industry with gaining the highest efficiency possible. Whereas a hydro turbine has a very smooth surface to minimize losses, a mass produced pump will often have a high level of roughness on the impeller.

Another key thing is that a centrifugal pump, compared to a regular hydro turbine, does not have any guide vanes. Whereas a regular hydro turbine can adjust incoming flow, and is able to perform efficiently for a range of flow rates, a PAT does not have this option [4]. This will enable regular hydro turbines to produce power at BEP, even through varying conditions. By implication, the range of suitable operating flow rates is much more limited for a PAT. One solution to this problem is to have multiple PATs coupled in series. With such a rig, one will be able to activate the number of pumps required to handle the incoming flow rate most efficiently. Having said that, a single PAT may perform close to maximum efficiency if a suitable pump is chosen for the given site conditions. Especially if the site has a close to fixed water supply throughout the year.

2.1. Performance of a Francis turbine

Using a pump as a turbine requires understanding of how the performance is found for a regular turbine. It will be of importance to apply this to the turbine mode of a PAT, in which the performance can be predicted. The turbine's runner will transform the available hydraulic energy to mechanical energy, and the hydraulic efficiency is a measure of how good this transformation is. The hydraulic efficiency is defined as:

$$\eta_{h,t} = \frac{u_{1,t}c_{u1,t} - u_{2,t}c_{u2,t}}{gH_{n,t}} \tag{1}$$

In equation 1, u is the peripheral velocity, while c_u is the peripheral component of the absolute velocity. Subscripts $1,t$ and $2,t$ refer to the inlet and outlet of the turbine, respectively. Furthermore, H_n is the available net head, while g is the acceleration due to gravity.

Assuming zero losses in the turbine, the hydraulic efficiency is $\eta_{h,t} = 1$, where the runner blades will have angles perfect for transforming hydraulic energy to mechanical [5]. As the turbine transforms hydraulic energy to mechanical energy, it works as a throttle in the system.

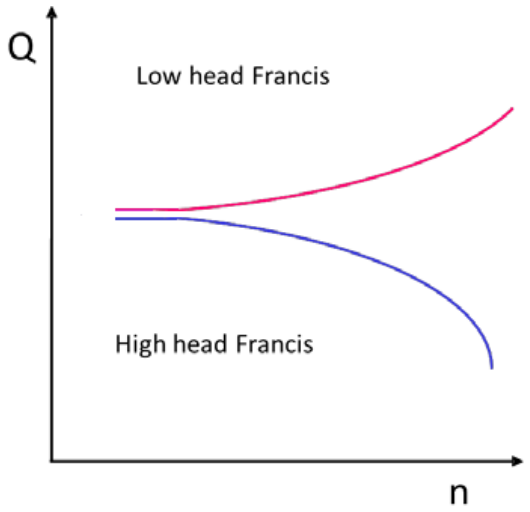

Figure 1: Showing the tendency of how the flow, Q, varies with the rotational speed, n, for low head and high head Francis turbines (Adapted from [5]).

Nielsen (2015)[5] shows that this throttling is a function of the rotational speed and depends on the geometry of the turbine, where the relationship between flow and rotational speed ($Q - n$) is dependent on the $D_{1,t}/D_{2,t}$-ratio. For high head Francis turbines, the flow has a tendency to decrease as a function of the rotational speed, seen in figure 1. Likewise, for low head turbines, where the $D_{1,t}/D_{2,t}$-ratio is low, the flow increases with n.

2.2. Earlier work

As the main disadvantage of a PAT is the difficulty of predicting the turbine characteristics that are needed for a given site, a lot of work has been done throughout the years to establish prediction methods which calculates the performance [6]. The actual turbine performance must be found through testing, but as this is a costly and time consuming process, as well as it requires that the pump has already been purchased, many different empirical correlations have been produced. These in turn produce a wide range of results. A common factor, however, is that the optimal operating point of a PAT is higher in both head and flow, than that of the pump it originates from [1]. This is to account for the head reduction caused by the various losses in turbine operation.

The two main approaches that has been taken to predict turbine performance are either using the pump efficiency, or by relating the head and flow ratios to the specific speed [6]. Williams (1994)[6] investigated in total eight different prediction techniques, and compared the accuracy of the models. Table 1 gives an outline of the different methods, as well as the appropriate relationship of the head correction factor $\tilde{h} = \frac{H_t}{H_p}$ and the discharge correction factor $\tilde{q} = \frac{Q_t}{Q_p}$.

According to Williams' (1994)[6] study, the method of Sharma proved to be the most accurate. The test involved comparing the turbine prediction methods on 35 different pumps, with available test data. As Sharma's method proved to be the most accurate, it is the only one that will be looked at here. He relates the discharge and head correction factors to the pump efficiency as shown in equations 2 and 3.

$$\tilde{q} = \frac{Q_t}{Q_p} = \frac{1}{\eta_p^{0.8}} \tag{2}$$

$$\tilde{h} = \frac{H_t}{H_p} = \frac{1}{\eta_p^{1.2}} \tag{3}$$

Even though a few of the other methods proved competitive, Sharma's method was found to be the most accurate of the eight approaches. Still, 20 percent of the tested pumps fell outside what was said to be the acceptable prediction limits. Therefore, it will always be wise to conduct thorough tests before installing a certain PAT [6]. Also, what is important to note, is that all these methods do only produce one best efficiency operating point, and not a full turbine characteristic.

Although the accuracy of the different correlations can be questioned, they may serve as a rough guide when designing a PAT-site [7]. However, the questionable precision, along with the large number of different pumps that need to be tested to create a trustworthy model, motivates a new approach. An approach in which the turbine performance is determined solely based on the pump geometry, as well as producing turbine characteristics on either side of the best efficiency point.

Table 1: Different prediction methods investigated by Williams (1994) [6].

Name of method/investigator	Based on	Head correction factor $\tilde{h}$	Discharge correction factor $\tilde{q}$
Childs	BEP	$\frac{1}{\eta_p}$	$\frac{1}{\eta_p}$
Hancock	BEP	$\frac{1}{\eta_t}$	$\frac{1}{\eta_t}$
Stepanoff	BEP	$\frac{1}{\eta_p}$	$\frac{1}{\sqrt{\eta_p}}$
Sharma	BEP	$\frac{1}{\eta_p^{1.2}}$	$\frac{1}{\eta_p^{0.8}}$
Alatorre-Frenk	BEP	$\frac{1}{0.85\eta_p^5+0.385}$	$\frac{0.85\eta_p^5+0.385}{2\eta_p^{9.5}+0.205}$
Schmiedl	BEP	$-1.4+\frac{2.5}{\eta_{hp}}$	$-1.5+\frac{2.4}{\eta_{hp}^2}$
Grover	Specific speed	$2.693-0.0229N_{st}$	$2.379-0.0264N_{st}$
Hergt	Specific speed	$1.3-\frac{6}{N_{st}-3}$	$1.3-\frac{1.6}{N_{st}-5}$

3. Methodology

The method presented in this study, takes a different approach than previous prediction techniques. It is based on assuming symmetry in the velocity diagram of a pump and a turbine. By this assumption, the inlet diagram of a turbine could be directly mirrored from the outlet diagram of a pump. The same procedure was then also applied to find the turbine outlet diagram, from the pump inlet diagram. The two respective diagrams and their mirrored opposites are presented in figure 2a and 2b. It is important to note that with this approach the slip and losses such as friction and shock losses, are not directly accounted for. This will be a topic of discussion later.

The BEP values of head and flow for a PAT can thus be calculated directly from any arbitrary centrifugal pump, provided that the pump geometry is known. This is information that can be troublesome to find, as it is not usually supplied by pump manufacturers. For this reason, professor Torbjørn K. Nielsen supplied a spreadsheet which calculates the main dimensions, and designs a centrifugal pump. From this, the main dimensions of the PAT such as diameters, heights, and angles can be taken directly from the pump dimensions. While doing so, extra care has to be taken when defining the inlet and outlet regions, as the outlet dimensions of the pump becomes the inlet dimensions of the turbine, and vice versa. Further, by using standard Francis

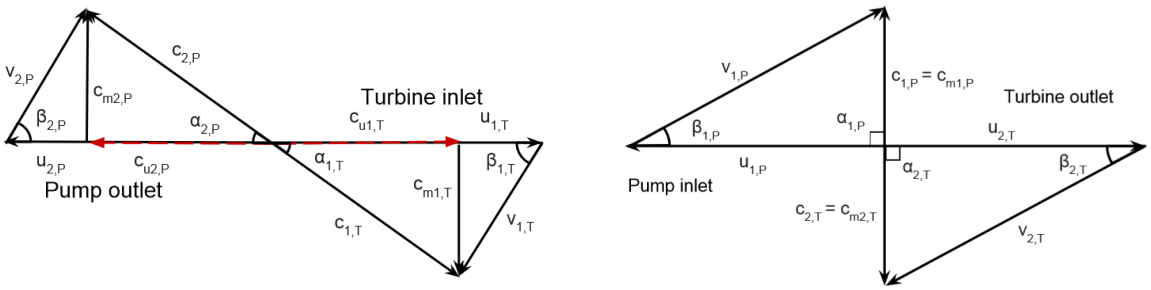

Figure 2: Obtaining the PAT velocity diagram by symmetry (not to scale).

turbine design equations, and assuming no rotation at the outlet, the rated values H_R and Q_R for the PAT were found. These values are factors of the rotational speed, which are specified to be the same in turbine mode as in pump mode. This is because it is of interest to use the pump motor as a generator for the PAT set up, to limit the capital costs even more.

3.1. Designing a Francis turbine

The geometry of a centrifugal pump is quite similar to that of a Francis runner, only with the fluid flowing in the opposite direction. Therefore, after applying the symmetry method, it was of interest to compare the PAT to a Francis turbine specifically designed for the same head and flow. Naturally, such a Francis turbine will have a different geometry than the PAT. When designing a Francis turbine at its best efficiency, one assumes that there is no rotation at the outlet, and c_{u2} was set to zero. Further, the hydraulic efficiency was assumed to be 0.96, and the reaction ratio $R = 0.5$ as it is common to assume that approximately 50% of the total net specific energy is converted to mechanical energy in the runner [8]. Knowing this, the following equation for the reaction ratio, taken from [8], could be applied:

$$R = 2\underline{u_{1,t}c_{u1,t}} - \underline{c_{u1,t}^2} \tag{4}$$

By recognizing the first term on the right hand side of equation 4 as the theoretical hydraulic efficiency, the reduced absolute tangential and peripheral velocities could be found. Then, together with the same values for rotational speed, head and flow as for the PAT's BEP values, the main dimensions of the Francis turbine were calculated. However, a few of the dimensions had to be assumed first. According to Brekke (2003)[8], it is common to choose a $\beta_{2,t}$ angle between 13°and 19°, and a $u_{2,t}$ component between 35 and 43 m/s. These are values that have proven adequate through years of experience. Therefore, when designing this fictional Francis runner, the chosen parameters were set to $\beta_{2,t} = 16°$ and $u_{2,t} = 40m/s$. It is also the norm to demand a slight acceleration of the meridional velocity component c_m through the runner, as an accelerating flow reduces the chance of a retardation. Thus, as $c_{m2,t}$ could be found through the angle and peripheral velocity stated above, $c_{m1,t}$ could be determined when assuming a 10% velocity increase from inlet to outlet.

3.2. Producing the PAT's $H-Q$ curve

Up until now it is only the performance at BEP that has been addressed. However, it is very much of interest to be able to predict how the PAT will perform at either side of this point. This is possible by manipulating the dimensionless momentum equation presented by Nielsen (2015)[5]:

$$T_{wt}\frac{dq}{dt} = h - \frac{q|q|}{\kappa^2} - \sigma(\tilde{\omega}^2 - 1) = 0 \tag{5}$$

In equation 5, T_{wt} is a time constant representing the hydraulic inertia, while q, h and $\tilde{\omega}$ are dimensionless properties for flow, head and angular speed respectively. Further, σ is the dimensionless throttling dependency of angular speed of rotation, and κ the opening degree of the turbine. A more thorough explanation of the method, as well as variable definitions, may be found in Appendix A.

Now, by varying the rotational speed n, and solving the stationary version of equation 5 for q, the discharge Q_t for different rotational speeds was found. IEC 62097 [9] specifies the two dimensionless factors for speed and discharge, shown in equation 6 and 7 respectively.

$$n_{ed} = \frac{nD_{2,t}}{\sqrt{gH_{R,t}}} \tag{6}$$

$$Q_{ed} = \frac{Q_t}{D_{2,t}^2\sqrt{gH_{R,t}}} \tag{7}$$

From these two equations the turbine's $Q_{ed} - n_{ed}$ relationship was established, and from this relationship the PAT's $H-Q$ curve was predicted.

For validation purposes, this approach was initially carried out for two different pumps. As the access to available pump geometries was limited, the geometries for the two different pumps were fictional, and calculated through the earlier mentioned design spreadsheet supplied by professor Torbjørn K. Nielsen. The method was tested for a radial high head pump, as well as a more axial pump with lower head. This was done in order to compare the resulting $Q_{ed} - n_{ed}$ and $H-Q$ curves to literature, and expected results.

In order to follow the outlined approach, and to assume symmetry in the pump outlet to the turbine inlet, only a few pump parameters are needed. The hydraulic efficiency was assumed to be 1. Additionally, the pump meridional velocity component, $c_{m1,p}$, is also an input parameter in the model. This value needed to be assumed. For the two fictional pumps the meridional velocity was prescribed a value of $c_{m1,p} = 9m/s$ based on Nielsen's assumptions. All other required input parameters are presented in table 2.

Table 2: Fictional pump geometry parameters and operating conditions.

Parameter	Pump 1	Pump 2	Unit
Inlet diameter $D_{1,p}$	1.457	1.5	m
Outlet diameter $D_{2,p}$	1.737	3	m
Outlet height $B_{2,p}$	0.284	0.3	m
Outlet blade angle $\beta_{2,p}$	12	12	°(degrees)
Inlet meridional velocity $c_{m1,p}$	9	9	m/s
Rotational speed n	600	600	rpm

3.3. Test-Pump 1

To be able to properly validate and verify the symmetry prediction method presented, experiments has to be carried out. These experiments are scheduled to be conducted in the laboratory at the University of Dar es Salaam, Tanzania and at NTNU. The PAT test rig in Dar es Salaam is equipped with two pumps, where one of them will work as a PAT. This is an old pump, where both the name and pump characteristic is unknown. However, it has been found that at its best efficiency in pump mode, it has a rated head of $H_{R,p} = 10m$ and flow $Q_{R,p} = 0.05m^3/s$. The symmetry method was therefore applied to this pump geometry, hereby referred to as *Test-Pump 1*. As this pump had a modest discharge, Q_p, compared to the two fictional pumps, the assumption of $c_{m1,p}$ needed to be adjusted in order to predict the turbine performance accurately. According to Bye (1967)[10], the absolute inlet velocity, $c_{1,p}$, can take the value of $2.3 - 5m/s$ for pumps at low discharge. As $c_{1,p} = c_{m1,p}$ at the pump inlet, the meridional velocity, $c_{m1,p}$ was set to $2.5m/s$ for this pump.

Test-Pump 2, which is the pump scheduled to be tested at NTNU, has been ordered from the manufacturer. However, the geometry data has not yet been measured. Therefore, further investigation in this paper will be on *Test-Pump 1*, where the most important pump parameters, the pump dimensions, as well as the operating conditions, are presented in table 3. It is important to remember that the input parameters for the pump become the outlet parameters for the PAT. Thus, one has to be careful not to adopt incorrect values.

Table 3: Geometry parameters and operating conditions of *Test-Pump 1*.

Parameter	Value	Unit
Inlet diameter $D_{1,p}$	148.1	mm
Outlet diameter $D_{2,p}$	197.3	mm
Outlet height $B_{2,p}$	34.3	mm
Outlet blade angle $\beta_{2,p}$	20.17	°(degrees)
Inlet meridional velocity $c_{m1,p}$	2.5	m/s
Rotational speed n	1450	rpm
Pump efficiency η_p	0.804	-

4. Results

4.1. Comparable results; PAT versus Francis turbine

By assuming symmetry in the velocity diagrams from the outlet of the pump to the inlet of the turbine, and using the pump's outlet dimensions as the inlet dimensions in turbine mode, the PAT characteristics at BEP could be determined. By obtaining the values for the rated flow and head, appropriate $Q_{ed} - n_{ed}$ and $H - Q$ curves were calculated. This was done in order to predict the PAT's performance outside of the best efficiency point. Further, it was of interest to design a Francis runner for the same head and flow as was found for the PAT. By doing so, conclusions could be drawn between the performance of a pump used as a turbine, and a Francis turbine specifically designed for certain conditions. This would also reveal some of the limitations of the PAT.

As mentioned previously, two different fictional pumps were used to produce the initial results. These consisted of both a high head pump, and one of lower head. The resulting BEP values for head and discharge in turbine mode were found to be $H_{R,t} = 44.5m$ and $Q_{R,t} = 15.3m^3/s$

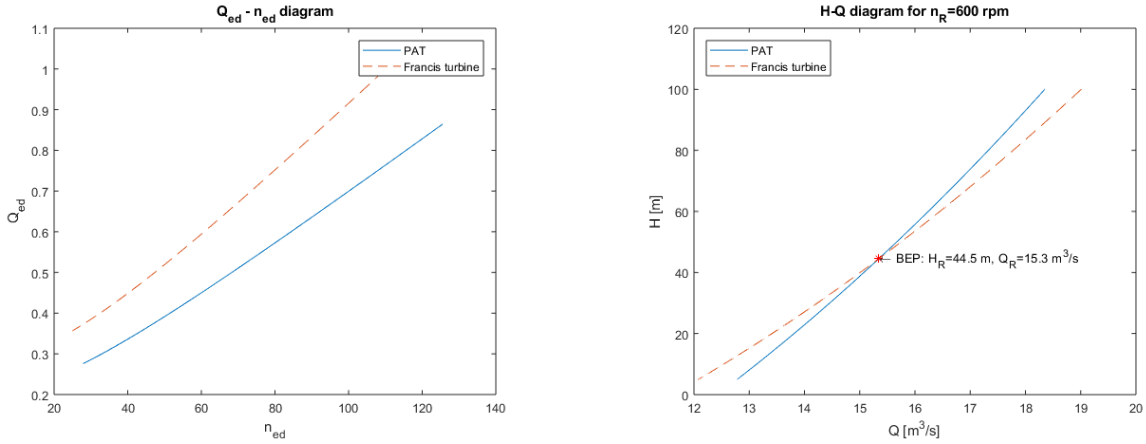

(a) (b)

Figure 3: $Q_{ed} - n_{ed}$ and $H - Q$ curves for $H_{R,t} = 44.5m$ and $Q_{R,t} = 15.3m^3/s$.

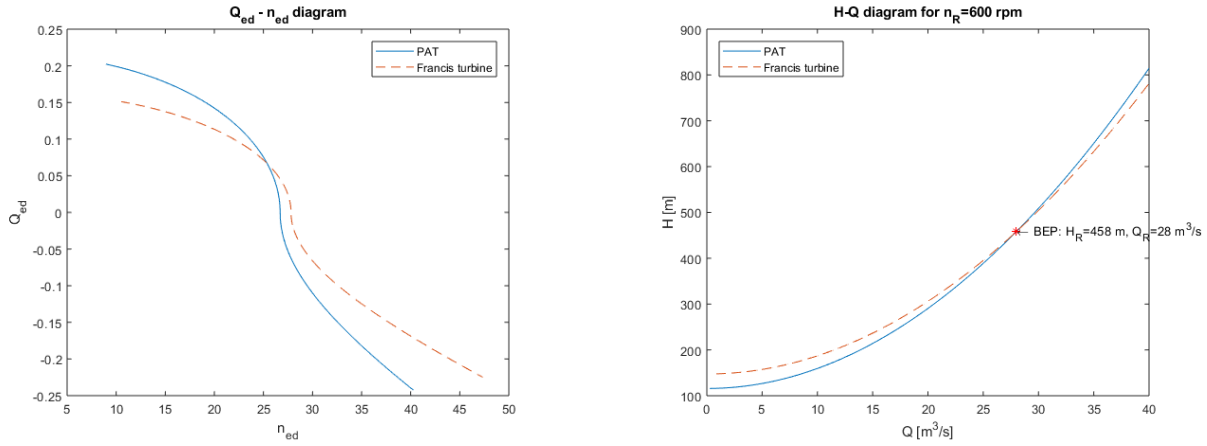

(a) (b)

Figure 4: $Q_{ed} - n_{ed}$ and $H - Q$ curves for $H_{R,t} = 458m$ and $Q_{R,t} = 28m^3/s$.

for the lower head case. For the high head case the equivalent BEP values were $H_{R,t} = 458m$ and $Q_{R,t} = 28m^3/s$. These results are summarized in table 4.

Table 4: Results of the two fictional PATs.

Parameter	PAT 1	PAT 2	Unit
Rated head $H_{R,t}$	44.5	458	m
Rated discharge $Q_{R,t}$	15.3	28	m^3/s
Speed number $^*\underline{\Omega}$	1.53	0.36	-

Figure 3a displays the $Q_{ed} - n_{ed}$ relationship for the lower head case, both for the PAT and the designed Francis turbine. From this result, the $H - Q$ curves presented in figure 3b was calculated. Similarly, figure 4a and 4b follow the same approach, but for the high head case.

4.2. Test-Pump 1

After seeing that the method behaved in a desired manner, further calculations were done on one specific pump, the one referred to as *Test-Pump 1*. With this geometry, as specified in table 3, the BEP values for head and discharge came out to be $H_{R,t} = 11.44m$ and $Q_{R,t} = 0.0585m^3/s$. Additionally, the speed number of this PAT was calculated to $\underline{^*\Omega} = 0.63$.

Table 5: Results of Test-Pump 1 working as a PAT.

Parameter	Test-Pump 1	Unit
Rated head $H_{R,t}$	11.44	m
Rated discharge $Q_{R,t}$	0.0585	m^3/s
Speed number $\underline{^*\Omega}$	0.63	$-$

In the same manner as for the two fictional PATs, the $Q_{ed} - n_{ed}$ and $H - Q$ curves were calculated based on the BEP values for *Test-Pump 1*. These are presented in figures 5a and 5b, respectively. These are the PAT characteristics that future test results will be compared up against.

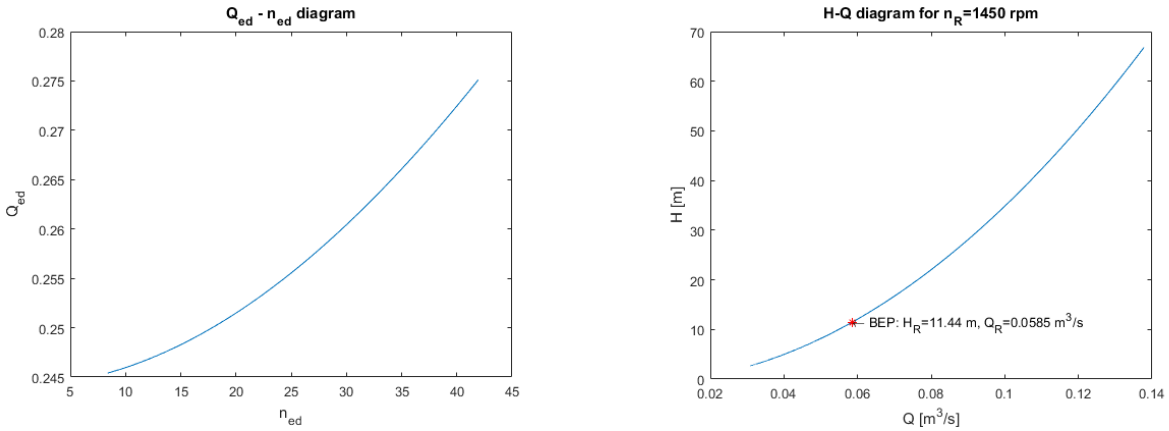

(a) (b)

Figure 5: $Q_{ed} - n_{ed}$ and $H - Q$ curves for *Test-Pump 1*.

4.3. Applying Sharma's prediction method to Test-Pump 1

To be able to conclude if this prediction method has any future, it was of great significance to compare it to the old empirical correlations. As Sharma's performance prediction method was found to be most accurate of the eight methods Williams (1994)[6] looked at, it was the only one considered here.

By equations 2 and 3, as well as the rated values for head and discharge for the pump at BEP, the PAT's performance at BEP could be calculated as follows:

$$H_t = \frac{H_p}{\eta_p^{1.2}} = \frac{10}{0.804^{1.2}} = 12.99m \tag{8}$$

$$Q_t = \frac{Q_p}{\eta_p^{0.8}} = \frac{0.05}{0.804^{0.8}} = 0.0595m^3/s \tag{9}$$

5. Discussion

5.1. PAT versus Francis turbine

By looking at the results presented for the two fictional PATs, it can be seen that the symmetry prediction model is in agreement with literature. The $Q_{ed} - n_{ed}$ diagrams in figures 3a and 4a follow the same speed-flow relationship as can be seen in figure 1. This can be observed for both the high head and lower head case. The $H - Q$ curves in figures 3b and 4b are also analogous in shape to what an authentic turbine may produce [8].

Taking a closer look at the lower head case in figure 3a, and comparing the PAT to a Francis turbine designed for the same BEP values of head and flow, it becomes clear that the PAT is inferior. The pump's angles and geometry makes the PAT less suitable in turbine mode than a Francis turbine, which in turn will result in a lower power production. For increasing speed values, the Francis turbine will be able to handle a higher discharge. Therefore, for the same rated head, the Francis runner will be able to produce more power. Also, as the Francis runner is expected to have a higher efficiency than the PAT, this tendency will be amplified.

For the high head case in figure 4a, the relationship is different. The PAT curve is significantly steeper than the curve for the Francis turbine. As the rotational speed increases to the point where Q_{ed} becomes negative, the flow changes direction. Past this point, the machines are working as pumps. This "pumping effect" is when the rotational speed is increased enough so that the fluid is throttled through the runner [11]. Naturally, the PAT will work better in this region, as it is a pump originally, and will handle larger flow values for a given rotational speed.

Additionally, for low speeds the PAT lies above the Francis turbine curve, which at first glance may be considered strange. This could be because of the geometry, where the relationship between inlet and outlet diameters make the PAT more radial than the Francis runner, and thus makes it better designed for high head values. However, this is only in the low speed region. At this point one may also draw a connection between a PAT and a reversible pump turbine (RPT), as they will have certain geometrical similarities. A RPT will have a similar $Q_{ed} - n_{ed}$ characteristic, as it too will be steeper than the Francis turbine [11].

The corresponding $H - Q$ curves are presented in figures 3b and 4b. They show a similar relationship for both cases, but with the high head case graphed for a larger discharge range. In both cases, the geometry, and $D_{1,t}/D_{2,t}$-ratio, make the PAT more radial than the Francis runner. This in turn makes the $H - Q$ curve steeper for the PAT. For the high head case, where the PAT is more radial than the low head, this effect is stronger, and the curve is even steeper.

An implication of this is that the PAT is harder to operate. As the head-flow relationship is steep, a slight change in any of the two variables will take the operation well away from its BEP. For a Francis turbine, this could be solved by modifying the guide vanes. But, for a PAT with no guide vanes, it is clear that this will have a considerable negative effect on the power production during varying conditions.

5.2. PAT characteristics of Test-Pump 1

By using the input parameters for the pump that is scheduled to be tested in Dar es Salaam, the applied method predicts characteristics as shown in figure 5. The best efficiency point in turbine mode was found to be at $H_{R,t} = 11.44m$ and $Q_{R,t} = 0.0585m^3/s$. In comparison, the rated head and flow in regular pump mode is $H_{R,p} = 10m$ and $Q_{R,p} = 0.05m^3/s$. Thus, the operation point at BEP lies higher, both for head and discharge, in PAT mode compared to pump mode. This is analogous to what has been stated previously.

To verify if the presented prediction method is within reasonable limits, the actual $H - Q$ performance of the PAT must be established in the laboratory. This will reveal the method's credibility, and if the assumptions have been acceptable.

5.3. Sharma's prediction method

The prediction method of Sharma estimated the PAT's best efficiency point to be at $H_{R,t} = 12.99m$ and $Q_{R,t} = 0.0595m^3/s$. As expected, this method also predicts BEP values for the PAT above pump BEP values. When comparing the symmetry prediction method outlined in this report, to that of Sharma's, it deviates 11.9% in head and 1.7% in discharge when looking at *Test-Pump 1*. At this stage, however, comparing the two prediction methods give limited closure. Therefore, it will be interesting to conduct proper test, and to compare the two methods to the real characteristic, for this specific pump.

Table 6: Prediction method comparison of *Test-Pump 1*: Sharma vs symmetry.

Parameter	Sharma	Symmetry	Deviation
Rated head $H_{R,t}$	$12.99m$	$11.44m$	11.9%
Rated discharge $Q_{R,t}$	$0.0595m^3/s$	$0.0585m^3/s$	1.7%

5.4. Assumptions, losses, and inaccuracies

A pitfall to the presented symmetry method is that the meridional velocity $c_{m1,p}$ has to be assumed. For *Test-Pump 1* this velocity was assumed to be $c_{m1,p} = 2.5m/s$, because of the modest amount of discharge. This assumption was based on numbers presented by Bye (1967)[10]. There are uncertainties related to this assumption, and the integrity of which may be questioned. Hence, if a range of different pumps are to be examined with this method, new meridional velocities have to be assumed. Therefore, it will be of interests to establish a more general criterion, and a better way to estimate this parameter. One possible solution may be to calculate the meridional velocity based on the flow and the geometry of the impeller inlet. However, the impeller inlet height was not available during the time of this study.

Another aspect that hasn't been addressed is the effect of friction and shock losses. In turbine mode, these losses will contribute to a reduction of the net head. Therefore, it might be expected that the actual BEP of the test-pump in PAT mode lies even higher than what has been predicted, to account for these losses. If these losses are quantified, the symmetry method may be used to create a span of BEP values. This span would range from zero losses, to a maximum amount of expected losses. Then, one could be more confident that the actual BEP lies within this interval.

Further, the assumption of total symmetry between pump and turbine mode may also be questioned. When applying symmetry, a decision was made not to include the slip from pump operation. Slip would have altered the blade angle to the relative flow angle, and consequently

changed the velocity diagram in turbine mode. This can be justified as the effect of slip in turbine operation, compared to pump operation, will be modest, and therefore may be neglected [12].

Finally, the hydraulic efficiency was for simplicity set to 1. Even though it has been proven that the efficiency of the PAT will be almost the same as in pump operation, the actual efficiency of a PAT will be significantly lower than 100%. The accuracy of the prediction method could therefore be enhanced by including a more realistic pump efficiency.

6. Conclusion

The objective was to investigate the possibility of predicting a PAT's performance, only given the pump's geometry. For this, a general method based on symmetry has been suggested. However, in addition to the measurable lengths and angles of the pump, a few assumptions had to be made. These may weaken the model, and contribute a more inaccurate prediction.

In order to be able to validate and verify the prediction model, tests are scheduled to be conducted. As these tests will be run on the pump referred to as *Test-Pump 1* at the University of Dar es Salaam, proposed characteristics of this pump were produced.

Several losses and uncertainties have been discussed as well, where the ones left out may very well have a substantial impact on the predicted characteristics. However, supported by literature, the predicted BEP points in turbine mode are higher than for pump mode. Also, by applying one of the established empirical prediction methods, it can be observed that the symmetry method follows the same trend.

Lastly, what remains is therefore to conduct the necessary tests for validation.

Appendix A. Producing the PATs H-Q curve

Start by manipulating the dimensionless momentum equation presented by Nielsen (2015)[5]:

$$T_{wt}\frac{dq}{dt} = h - \frac{q|q|}{\kappa^2} - \sigma(\tilde{\omega}^2 - 1) = 0 \tag{A.1}$$

Where T_{wt} is a time constant representing the hydraulic inertia. This value was not needed however, as the left hand side of the equation could be set to zero to find the stationary characteristic. Furthermore, the dimensionless properties for flow, head and angular speed of rotation in equation A.1 are defined as $q = Q_t/Q_{R,t}$, $h = H_t/H_{R,t}$ and $\tilde{\omega} = \omega/\omega_R$. Now, by assuming that the PAT has BEP at $q = 1$, $h = 1$, $\tilde{\omega} = 1$, and that the derivative of the hydraulic efficiency in the Euler turbine equation (1) with regards to ω is zero, $\partial\eta/\partial\omega = 0$, the PAT's dimensionless throttling dependency of angular speed of rotation, σ, is defined as seen in equation A.2.

$$\sigma = \frac{\eta_{hR} - \psi}{\eta_{hR} + \psi} \tag{A.2}$$

By setting the hydraulic efficiency, $\eta_{hR} = 1$ for BEP in equation A.2, and defining the machine coefficient as

$$\psi = \frac{{u_{2,t}}^2}{gH_{R,t}}, \tag{A.3}$$

σ for the PAT could be found. Further, the opening degree of the turbine, κ, equals 1 for the BEP, and is defined by:

$$\kappa = \frac{\frac{Q_t}{\sqrt{2gH_t}}}{\frac{Q_{R,t}}{\sqrt{2gH_{R,t}}}} \tag{A.4}$$

By varying the rotational speed n, and solving the stationary version of equation A.1 for q, the discharge Q_t for different rotational speeds were readily found. IEC 62097 [9] specifies the two dimensionless factors for speed and discharge, shown in equation A.5 and A.6 respectively.

$$n_{ed} = \frac{nD_{2,t}}{\sqrt{gH_{R,t}}} \tag{A.5}$$

$$Q_{ed} = \frac{Q_t}{D_{2,t}^2\sqrt{gH_{R,t}}} \tag{A.6}$$

From these two equations the turbine's $Q_{ed} - n_{ed}$ relationship was established. The $H - Q$ curve could then be produced by first solving equation A.5 for H_t:

$$H_t = \frac{(\frac{nD_{2,t}}{n_{ed}})^2}{g} \tag{A.7}$$

By keeping the rotational speed constant, and only varying the speed factor, H_t was found. Finally, the definition of the discharge factor was modified to equation A.8 to give a result for Q_t for changing values of Q_{ed} and corresponding H_t. This enabled graphing of the turbine's $H - Q$ relationship.

$$Q_t = Q_{ed}D_{2,t}^2\sqrt{gH_t} \tag{A.8}$$

References

[1] Jain S V and Patel R N 2014 *Renewable and Sustainable Energy Reviews* **30** 841–868
[2] Williams A 1996 *Renewable Energy* **9** 1227–1234
[3] Fernandez J, Blanco E, Parrondo J, Stickland M and Scanlon T 2004 *Proceedings of the Institution of Mechanical Engineers, Part A: Journal of Power and Energy* **218** 265–271
[4] Williams A *et al.* 1995 *Pumps as turbines: a user's guide* (Intermediate Technology)
[5] Nielsen T K 2015 *International Journal of Fluid Machinery and Systems* **8** 169–182
[6] Williams A 1994 *Proceedings of the Institution of Mechanical Engineers, Part A: Journal of Power and Energy* **208** 59–66
[7] Teuteberg B H 2010 *Design of a pump-as-turbine microhydro system for an abalone farm* Ph.D. thesis Stellenbosch: University of Stellenbosch
[8] Brekke H 2003 *Vannkraftlaboratoriet NTNU*
[9] IEC62097 2009 *Hydraulic machines, radial and axial - Performance conversion method from model to prototype*
[10] Bye G 1967 *Pumper:(Omsl.: Elmer Rodin)* (Universitetsforlaget)
[11] Nielsen T K and Olimstad G
[12] Chapallaz J M, Eichenberger P and Fischer G 1992 *Manual on pumps used as turbines* (Vieweg)

APPENDIX B

Calibration and Uncertainty Analysis

When calibrating an instrument, different sources of error leads to the total uncertainty. Table B.1 describes the possible errors defined by IEC 60193 [16]. To find the total uncertainty, all the different uncertainties are combined in the *Root-sum-square* (RSS) method, presented in equation B.6.

Table B.1: Component errors in the calibration of an instrument.

Uncertainty	Description
$\pm f_{X_a}$	Systematic error in primary calibration method
$\pm f_{X_b}$	Random error in primary calibration method
$\pm f_{X_c}$	Systematic error (repeatability) of the secondary instrument
$\pm f_{X_d}$	Random error of the secondary instrument
$\pm f_{X_e}$	Physical phenomena and external influences
$\pm f_{X_f}$	Error in physical properties

B.1 Pressure sensors

Both the upstream and downstream pressure transducers were calibrated using a calibration hand pump, a *Druck DPI 601*. The primary calibrator uncertainty, thus the hand pump uncertainty, was found in calibration report B.8.1. For calibration of the transducers, a LabView program was utilized, which calculated the sensor regression line, as well as the systematic and random error in the calibrations.

The pressure sensor used upstream of the PAT was a *GE UNIK5000* transducer, ranging from $0-5\ bar\ gage$. Its calibration report can be found in B.8.4. The uncertainties for the upstream pressure transducer are shown in table B.2.

Table B.2: Calibration uncertainties for pressure transducer upstream of the PAT.

Uncertainty	Description	Magnitude
$f_{P_{1,a}}$	Systematic error in pressure calibrator	±0.050%
$f_{P_{1,regression}}$	Systematic and random error in instrument	$max(\pm 0.492\%)$

From this, the total calibration uncertainty for the upstream pressure transducer is found through the RSS method:

$$max(f_{P_{1,cal}}) = \pm\sqrt{(0.050)^2 + (0.492)^2} = \pm 0.495\% \tag{B.1}$$

The pressure sensor used downstream of the PAT was a *Druck PTX1400* transducer, ranging from $0-4\ bar\ gage$. The calibration report for this sensor is found in B.8.3. The uncertainties of this pressure transducer are shown in table B.3.

Table B.3: Calibration uncertainties for pressure transducer downstream of the PAT.

Uncertainty	Description	Magnitude
$f_{P_{2,a}}$	Systematic error in pressure calibrator	±0.050%
$f_{P_{2,regression}}$	Systematic and random error in instrument	$max(\pm 1.153\%)$

The table above gives the total calibration uncertainty of the downstream pressure trans-

ducer as:

$$max(f_{P_{2,cal}}) = \pm\sqrt{(0.050)^2 + (1.153)^2} = \pm 1.154\% \tag{B.2}$$

B.2 Flow sensor

For the PAT-experiment, an *OPTIFLUX 2000C* 50mm flow sensor was utilized. The calibration of this flow sensor was done at a previous point in time, and the report can be found in B.8.2. In the report, both systematic and random error in the primary instrument, a piston prover, as well as the systematic and random error in the secondary instrument, the flow sensor, can be found. The specific uncertainties are tabulated in table B.4.

Table B.4: Calibration uncertainties of the flow sensor.

Uncertainty	Description	Magnitude
$f_{Q_{ab}}$	Systematic and random error in piston prover	±0.020%
$f_{Q_{regression}}$	Systematic and random error in instrument	$max(\pm 0.23\%)$

Thus, the total calibration uncertainty becomes:

$$max(f_{Qcal}) = \pm\sqrt{(0.020)^2 + (0.23)^2} = \pm 0.231\% \tag{B.3}$$

B.3 Torque sensor

The sensor used for measuring the torque at the shaft, was an *HBM T22/200NM* transducer. In table B.5, the uncertainties have been estimated for the calibration in both pump and turbine mode. It was calibrated by applying torque to the shaft, where the direction differed from pump and turbine operation. This was done by connecting a horizontal metal bar to the shaft. A weight bed was connected to the bar via a wire so that the torque could be measured by adding weights to the weight bed. In reports B.8.5 and B.8.6, the calibration certificates can be found. The systematic error in weights and weight bed, as well as the systematic error in the length of the arm, was assumed as ±0.01% and ±0.013%, according to [17], respectively.

Table B.5: Calibration uncertainties for the torque sensor in both pump and turbine operation.

Uncertainty	Description	Magnitude
f_{τ_W}	Systematic error in weights and weight bed	±0.01%
$f_{\tau_{arm}}$	Systematic error in the length of the arm	$max(\pm 0.013\%)$
$f_{\tau_{regression,pump}}$	Systematic and random error in the instrument	$max(\pm 1.776839\%)$
$f_{\tau_{regression,PAT}}$	Systematic and random error in the instrument	$max(\pm 0.563075\%)$

The maximum calibration uncertainty is found by combining these errors, and equation B.4 and B.5 present the torque's uncertainty in pump and PAT operation, respectively:

$$max(f_{\tau_{cal,pump}}) = \pm\sqrt{(0.01)^2 + (0.013)^2 + (1.776839)^2} = \pm 1.7769\% \tag{B.4}$$

$$max(f_{\tau_{cal,PAT}}) = \pm\sqrt{(0.01)^2 + (0.013)^2 + (0.563075)^2} = \pm 0.5633\% \tag{B.5}$$

B.4 RPM sensor

The rotational speed was measured with an optical sensor, and a piece of reflective tape, taped to the shaft. The uncertainty of the measurements are assumed to be ±0.025%, as recommended by IEC 60193 [16].

B.5 Temperature sensor

A thermometer was used to measure the water temperature in order to find a tabulated density values. However, the systematic error of estimating the density is in order of ±0.01%, which is not significant in the total uncertainty of the derived parameters, and is therefore neglected [18].

B.6 Uncertainty of derived values

By using Gauss' law of error propagation, the uncertainty of derived parameters such as head and efficiency can be found. The error ΔY caused by the individual errors Δx_i is calculated as

seen below:

$$\Delta Y = \pm\sqrt{\left(\frac{\delta y_1}{\delta x_1}\Delta x_1\right)^2 + \left(\frac{\delta y_2}{\delta x_2}\Delta x_2\right)^2 + ... + \left(\frac{\delta y_n}{\delta x_n}\Delta x_n\right)^2} \tag{B.6}$$

where variable $Y = Y + \Delta Y$ is a function of $x_1, x_2, ...x_n$, such that

$$Y = y(x_1 \pm \Delta x_1, x_2 \pm \Delta x_2, ..., x_n \pm \Delta x_n) \tag{B.7}$$

The uncertainty is here given by $f_Y = \frac{\Delta Y}{Y}$. The uncertainty of the density of water is assumed negligible for the following calculations, because, as stated above, it is not significant in the total uncertainty of the derived parameters [18].

B.6.1 Pressure head

The pressure head is calculated by the use of Bernoulli's equation:

$$H = \frac{\Delta p}{\rho g} + \frac{Q^2\left(\frac{1}{A_{in}^2 - A_{out}^2}\right)}{2g} + \Delta z = \frac{\Delta p}{\rho g} + \frac{Q^2}{2ag} + \Delta z \tag{B.8}$$

where, in turbine operation, $\Delta p = p_{in} - p_{out}$, $\Delta z = z_{in} - z_{out}$, and $a = \frac{(A_{out}A_{in})^2}{A_{out}^2 - A_{in}^2}$. From this point on, the notation will change from $\Delta p = P$ and $\Delta z = Z$. The error in the height difference Z is found by assuming an error of $\pm 0.1mm$ when measured by a ruler. In this experiment, Δz was found to be $0.37m$, and therefore $f_z = \frac{0.1mm}{370mm} = \pm 0.027\%$. The total error in head is then given as:

$$\Delta H = \pm\sqrt{\left(\frac{\delta H}{\delta P}\Delta P\right)^2 + \left(\frac{\delta H}{\delta Q}\Delta Q\right)^2 + \left(\frac{\delta H}{\delta Z}\Delta Z\right)^2} = \pm\sqrt{\left(\frac{1}{\rho g}\Delta P\right)^2 + \left(\frac{Q}{ag}\Delta Q\right)^2 + \Delta Z^2} \tag{B.9}$$

The uncertainty of the pressure head is then calculated as follows.

$$f_H = \frac{\Delta H}{H} = \pm\sqrt{\frac{\left(\frac{1}{\rho g}\Delta P\right)^2 + \left(\frac{Q}{ag}\Delta Q\right)^2 + \Delta Z^2}{\left(\frac{P}{\rho g} + \frac{Q^2}{2ag} + Z\right)^2}} = \pm\sqrt{\frac{\left(\frac{1}{\rho g}\Delta P\right)^2 + \left(\frac{Q}{ag}\Delta Q\right)^2 + \Delta Z^2}{\frac{P^2}{\rho^2 g^2} + \frac{PQ^2}{\rho a g^2} + \frac{2PZ}{\rho g} + \frac{Q^4}{4a^2 g^2} + \frac{Q^2 Z}{ag} + Z^2}}$$

$$= \pm\sqrt{\frac{\frac{1}{\rho^2 g^2 Q^4 Z^2}\left(\frac{\Delta P}{P}\right)^2 + \frac{1}{P^2 a^2 g^2 Z^2}\left(\frac{\Delta Q}{Q}\right)^2 + \left(\frac{1}{P^2 Q^4}\right)\left(\frac{\Delta Z}{Z}\right)^2}{\frac{1}{Q^4\rho^2 Z^2 g^2} + \frac{1}{PQ^2 Z^2 \rho a g^2} + \frac{2}{PQ^4 Z\rho g} + \frac{1}{4P^2 Z^2 a^2 g^2} + \frac{1}{P^2 Q^2 Z a g} + \frac{1}{Q^4 P^2}}} \tag{B.10}$$

By inserting $f_P = \frac{\Delta P}{P}$, $f_Q = \frac{\Delta Q}{Q}$ and $f_P = \frac{\Delta Z}{Z}$, the expression turns to:

$$f_H = \pm\sqrt{\frac{P^2 a^2 {f_p}^2 + Q^4 \rho^2 {f_Q}^2 + Z^2 \rho^2 g^2 a^2 {f_Z}^2}{P^2 a^2 + PQ^2 \rho a + 2PZ\rho g a^2 + \frac{1}{4}Q^4\rho^2 + Q^2 Z\rho^2 a g + Z^2\rho^2 g^2 a^2}} \tag{B.11}$$

Note: $f_P = \sqrt{(f_{P1})^2 + (f_{P2})^2}$.

By inserting the values of f_P, f_Q and f_Z, as well as measured values for P, Q and Z, equation B.11, can be calculated to find the total uncertainty of the pressure head.

B.6.2 Efficiency

A similar uncertainty derivation as above is also needed for efficiency calculations. However, as the initial approach of measuring the power from the shaft torque was not feasible, this has been left out. Instead, an attempt was made in order to quantify the uncertainty in the manual reading of the power from the frequency converter display. Based on the variation in the power magnitude, an uncertainty of ±5% in the efficiency calculation was assumed.

B.7 Uncertainty from measurements

The error of a measurement is defined as the difference between the measured value and the actual value of the physical property [17]. In this analysis three types of errors have been considered - spurious errors, systematic errors and random errors.

Spurious errors are errors caused by human failures in an experiment, or by a failure in the measuring equipment itself. If some points in the measurement series is out of line with the rest of the measurements, they may be rejected [17]. Such points are called outliers. Systematic errors exists when using poorly calibrated instruments, and some of the sources of uncertainty are hysteresis and linearity issues in the instrument. It is therefore important to have enough measurement points in the calibration, to limit these errors.

Random errors come from repeatability, or test-retest reliability, and is the phenomenon when an instrument's output varies for the same measurement conditions, namely the same input [17]. When the number of measurements is large, the error may be found by using a Student-t distribution in order to describe the distribution around the mean. The Student-t distribution is quite similar in shape to a normal distribution, given that the number of measurement points is high, but the ends are spread more when the number of samples is low.

The expression for the confidence interval of the mean of the measurement with a $1-\alpha$ confidence is shown in equation B.12 [17].

$$P\left(\bar{X} - t_{\frac{\alpha}{2}}\frac{S_X}{\sqrt{N}} \leq \mu \leq \bar{X} + t_{\frac{\alpha}{2}}\frac{S_X}{\sqrt{N}}\right) = 1-\alpha \tag{B.12}$$

With S_X defined as

$$S_X = \sqrt{\frac{1}{N-1}\sum_{i=1}^{N}(x_i - \bar{X})^2} \tag{B.13}$$

where N is the number of samples and $t_{\alpha/2}$ is the t-value for the Student-t distribution with the confidence level of $1-\alpha$. In this study α was set to 5%.

B.8 Calibration certificates

B.8.1 Calibration certificate Druck DPI601

ITE Vannkrftlaboratoriet
NTNU 4539-1 ORIGINAL

Druck

CALIBRATION CERTIFICATE
(POSITIVE PRESSURE)

PAGE 1 OF 1

UNIT UNDER TEST (UUT)

Manufacturer	: Druck
Type Number	: DPI601
Serial Number	: 14206/96-1
Sales Order Number	: M11798-1
Parameter Range	: 0 to 10 bar g
Calibration Date	: 24 January 1996
Calibrated By	: S.Pattison
External Sensor Serial No.	:

CALIBRATOR INFORMATION

1.	Manufacturer	: Budenburg
	Calibration Instrument	: Type 246
	Serial Number	: 10442
	Calibrated Against (*1)	: Druck Stds. Lab.
	Pressure Medium	: Dry Nitrogen

AMBIENT CONDITIONS

Ambient Temperature (°C)	: 19.0
Local Gravity (ms^{-2})	: 9.81291

PERFORMANCE DATA

Nominal Applied Value bar	Actual Applied Value bar (*2)	Unit Under Test Reading bar (*3)	Unit Under Test Deviation (*4)	Permissible Deviation	Pass/ Fail
0.000	0.000	0.000	0.000 %fs	± 0.050%fs ± 1 digit	Pass
2.000	2.000	2.000	0.000 %fs	± 0.050%fs ± 1 digit	Pass
4.000	4.000	4.000	0.000 %fs	± 0.050%fs ± 1 digit	Pass
6.000	6.000	6.000	0.000 %fs	± 0.050%fs ± 1 digit	Pass
8.002	8.002	8.001	- 0.010 %fs	± 0.050%fs ± 1 digit	Pass
10.002	10.002	10.003	0.010 %fs	± 0.050%fs ± 1 digit	Pass

COMMENTS

I hereby certify that the details above are correct.

Certified by: S PATTISON Signed: S Pattison Date: 24 January 1996

NOTES

(*1) Traceable to relevant International Standards.
(*2) Actual Applied Value corrected for gravity and temperature as appropriate.
Where applicable, other scales to BS350 calculated equivalent engineering units are used.
(*3) Actual recorded values. For specification, see Permissible Deviation column.
(*4) Deviation calculated from U.U.T. Reading minus Actual Applied Value.

CAL1 6/92

Druck Limited, Fir Tree Lane, Groby, Leicester, LE6 0FH. Telephone (0116) 2314314, Telex: 341743 Druck G, Facsimile: (0116) 2875022.

B.8.2 Calibration certificate OPTIFLUX 2000 C

KROHNE

Calibration certificate

S/N : A07 00394 Project : 255200 10 1

Flow sensor:

Type:	OPTIFLUX 2000 C	GK:	2.3737
DN:	50 mm/ 2 inch	GKL:	4.4985
Flanges:	DIN2501 PN40		
Test pressure:	60 Bar	Field frequency:	Line frequency / 6
Liner:	Polypropylene		
Electrode constr.:	Standard		
Electrode material:	Hastelloy C4		
Protection class:	IP66 / 67		

The flow sensor has been calibrated against a piston-prover. The calibration certificate of this prover documents the traceability to national standards, which realize the physical units of measurements according to the International System of Units (SI). Uncertainty of the piston-prover is 0.02%

The results:

Calibration measuring range (100 %) : 21.2060 m^3/h

Flow in %	Deviation in %
98.62	-0.150
21.77	0.230

Dordrecht, 2007-02-12

Printserver 1.0.1179, PST 11

KROHNE Altometer, Kerkeplaat 12, 3313 LC Dordrecht, The Netherlands, Tel.: +31 (0)78 6306 300, Fax: +31 (0)78 6306 390, www.krohne.com

B.8.3 Calibration certificate Druck PTX 1400

DruckPTX1400kalibrering 24.04.18

CALIBRATION REPORT

CALIBRATION PROPERTIES

Calibrated by: Sondre Skjoldli, Øyvind Albert
Type/Producer: Druck PTX 1400
SN: Z00227/07
Range: 0-2,5 bar g
Unit: Bar

CALIBRATION SOURCE PROPERTIES

Type/Producer: Druck DPI601
SN: 14206/96-1
Uncertainty [%]: 0,05

POLY FIT EQUATION:

Y= -106,73877956E+0X^0 + 50,04254576E+0X^1

CALIBRATION SUMARY:

Max Uncertainty : 1,153234 [%]
Max Uncertainty : 0,442137 [Bar]
RSQ : 0,999966
Calibration points : 20

Figure 1 : Calibration chart (The uncertainty band is multiplied by 10)

COMMENTS:

Atmospheric Pressure when calibrated: 98,538 kPa

The uncertainty is calculated with 95% confidence. The uncertainty includes the randomness in the calibrated instrument during the calibration, systematic uncertainty in the instrument or property which the instrument under calibration is compared with (dead weight manometer, calibrated weights etc.), and due to regression analysis to fit the calibration points to a linear calibration equation. The calculated uncertainty can be used as the total systematic uncertainty of the calibrated instrument with the given calibration equation.

_____

Sondre Skjoldli, Øyvind Albert

B.8.4 Calibration certificate GE UNIK 5000

GEUNIK5000kalibrering 24.04.18

CALIBRATION REPORT

CALIBRATION PROPERTIES
Calibrated by: Sondre Skjoldli, Øyvind Albert
Type/Producer: GE UNIK 5000
SN: 4321073
Range: 0-2,5 bar g
Unit: Bar

CALIBRATION SOURCE PROPERTIES
Type/Producer: Druck DPI601
SN: 14206/96-1
Uncertainty [%]: 0,05

POLY FIT EQUATION:
Y= -125,51513139E+0X^0 + 62,47049663E+0X^1

CALIBRATION SUMARY:
Max Uncertainty : 0,491605 [%]
Max Uncertainty : 0,127840 [Bar]
RSQ : 1,000000
Calibration points : 20

Figure 1 : Calibration chart (The uncertainty band is multiplied by 10)

COMMENTS
Atmospheric Pressure when calibrated: 98,538 kPa

The uncertainty is calculated with 95% confidence. The uncertainty includes the randomness in the calibrated instrument during the calibration, systematic uncertainty in the instrument or property which the instrument under calibration is compared with (dead weight manometer, calibrated weights etc.), and due to regression analysis to fit the calibration points to a linear calibration equation. The calculated uncertainty can be used as the total systematic uncertainty of the calibrated instrument with the given calibration equation.

_____
Sondre Skjoldli, Øyvind Albert

B.8.5 Calibration certificate HBM T22 for pump operation

Torque pump operation

CALIBRATION REPORT

CALIBRATION PROPERTIES
Calibrated by: Sondre Skjoldli and Øyvind Albert
Type/Producer: HBM T22/200NM
SN: 01709720
Range: 4-37,5
Unit: Nm

CALIBRATION SOURCE PROPERTIES
Type/Producer: Calibrated Weights
SN: -
Uncertainty [%]: -

POLY FIT EQUATION:
Y= + 1,32395301E+0X^0 + 40,22771287E+0X^1

CALIBRATION SUMARY:
Max Uncertainty : 1,776839 [%]
Max Uncertainty : 0,078748 [Nm]
RSQ : 0,999871
Calibration points : 35

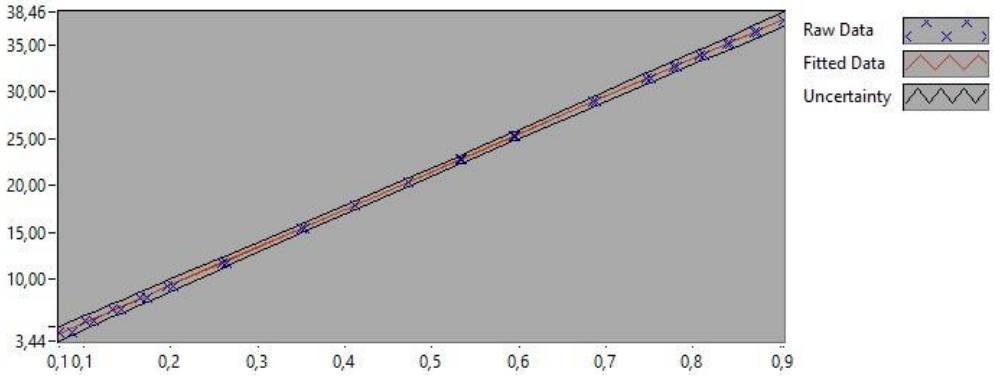

Figure 1 : Calibration chart (The uncertainty band is multiplied by 10)

The uncertainty is calculated with 95% confidence. The uncertainty includes the randomness in the calibrated instrument during the calibration, systematic uncertainty in the instrument or property which the instrument under calibration is compared with (dead weight manometer, calibrated weights etc.), and due to regression analysis to fit the calibration points to a linear calibration equation. The calculated uncertainty can be used as the total systematic uncertainty of the calibrated instrument with the given calibration equation.

Sondre Skjoldli and Øyvind Albert

B.8.6 Calibration certificate HBM T22 for turbine operation

Torque turbine operation

CALIBRATION REPORT

CALIBRATION PROPERTIES
Calibrated by: Sondre Skjoldli and Øyvind Albert
Type/Producer: HBM T22/200NM
SN: 01709720
Range: 4-37,5
Unit: Nm

CALIBRATION SOURCE PROPERTIES
Type/Producer: Calibrated Weights
SN: -
Uncertainty [%]: -

POLY FIT EQUATION:
Y= -1,33051734E+0X^0 - 40,31310084E+0X^1

CALIBRATION SUMARY:
Max Uncertainty : 0,563075 [%]
Max Uncertainty : 0,024987 [Nm]
RSQ : 0,999988
Calibration points : 34

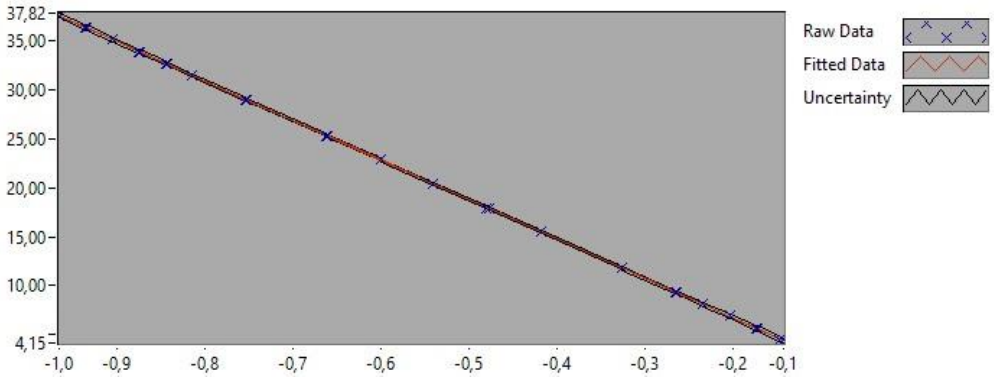

Figure 1 : Calibration chart (The uncertainty band is multiplied by 10)

The uncertainty is calculated with 95% confidence. The uncertainty includes the randomness in the calibrated instrument during the calibration, systematic uncertainty in the instrument or property which the instrument under calibration is compared with (dead weight manometer, calibrated weights etc.), and due to regression analysis to fit the calibration points to a linear calibration equation. The calculated uncertainty can be used as the total systematic uncertainty of the calibrated instrument with the given calibration equation.

Sondre Skjoldli and Øyvind Albert

APPENDIX C

LabVIEW

C.1 Front panel and block diagram

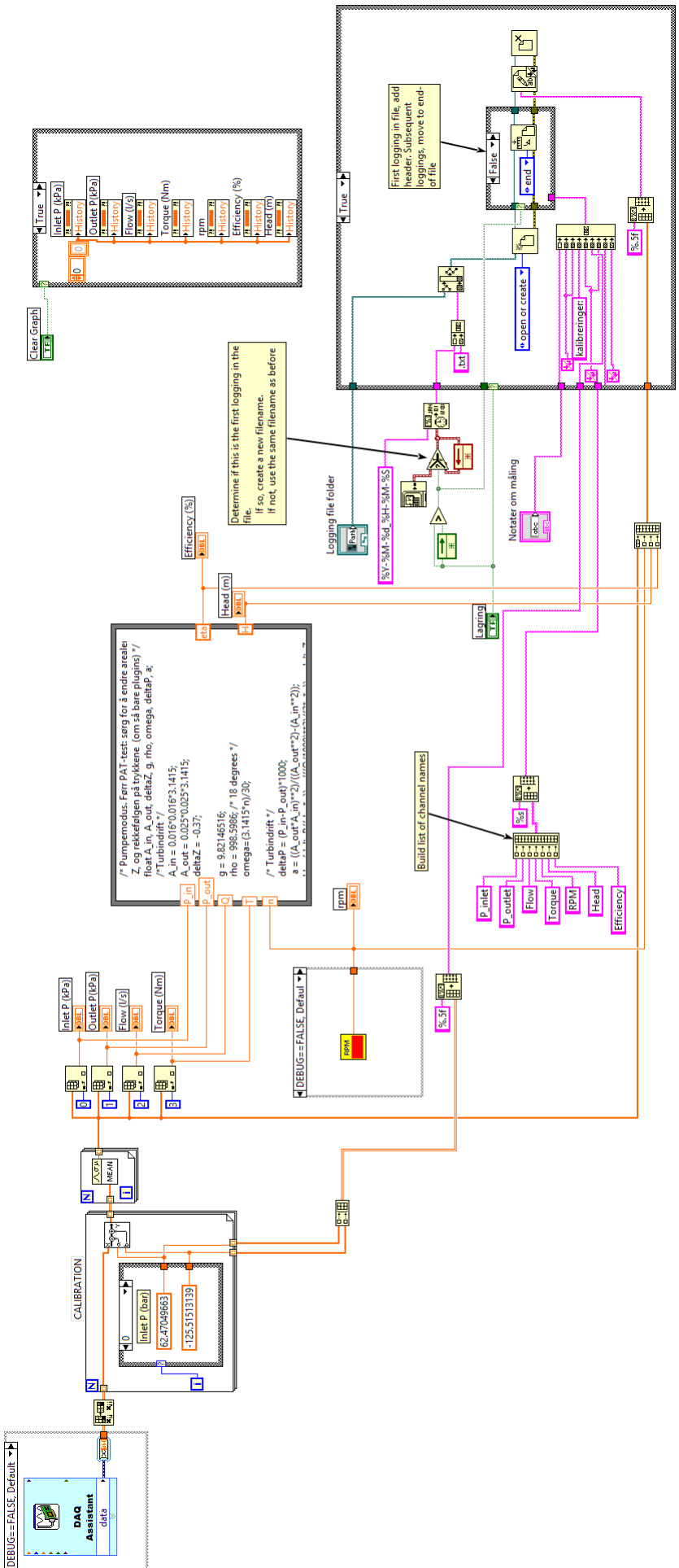
First logging in file, add header. Subsequent loggings, move to end-of file
Determine if this is the first logging in the file:
If so, create a new filename.
If not, use the same filename as before
Logging file folder
Notater om måling
Build list of channel names
CALIBRATION
DEBUG==FALSE, Default
DAQ Assistant
Clear Graph
Inlet P (kPa)
Outlet P(kPa)
Flow (l/s)
Torque (Nm)
rpm
Efficiency (%)
Head (m)
P_inlet
P_outlet
Flow
Torque
RPM
Head
Efficiency

APPENDIX D

Matlab codes

D.1 PAT prediction and experimental results compared

```
clear all
clc
close all

g=9.82146516;
rho = 998.5986;
Ain = pi*(0.032^2)/4;
Aout = pi*(0.05^2)/4;
a = (Aout*Ain)^2/(Aout^2-Ain^2); %In turbine mode
Z = -0.37; %In turbine mode

%Pump input parameters (efficiency assumed eta=1)
n_R=1450; %Rated rotational speed
D1P=0.051; %Inlet diameter
D2P=0.153; %Outlet diameter
B1P=0.0304; %For    regne ut cmlp
beta2P=29; %mean([29.5, 29.25, 28, 29.75, 29, 28.75]) %Blade angle
B2P=0.005; %Outlet height

%Empirical correlations
eta_pump = 0.58; %XX
```

```
eta_h_pump = 0;
H_pump = 5.75; %XX
Q_pump = 0.0025; %XX

%Calculated pump parameters
cm1P=Q_pump/(pi*D1P*B1P);
omega_R=(2*pi*n_R)/60;
u2P=(omega_R*D2P)/2;
%cm2P=1.1*cm1P;
cm2P=2.03*cm1P;
cu2P=u2P-(cm2P/tan(beta2P*pi/180));
alpha2P=atan(cm2P/cu2P)*(180/pi);

%PAT calculated values
D1=D2P;
D2=D1P;
B1=B2P;
beta1=beta2P;
u1=omega_R*(D1/2);
cm1=cm2P;
cu1 = cu2P;
alpha1=atan(cm1/cu1)*(180/pi);
u2=omega_R*(D2/2);
H_R=u1*cu1/g;
Q_R=cm1*pi*D1*B1;
phi=(u2^2)/(g*H_R);
sigma=(1-phi)/(1+phi);

n=[950:1:2150];
%PAT
for i=1:length(n)
    if (1-(sigma*((n(i)/n_R)^2-1)))<0
        q(i)=-sqrt(abs(1-(sigma*((n(i)/n_R)^2-1))));
        Q(i)=q(i)*Q_R;
        n_ed(i)=n(i)*(D2/sqrt(g*H_R));
        Q_ed(i)=Q(i)/(D2^2*sqrt(g*H_R));
        H(i)=(((n_R*D2)/n_ed(i))^2)/g;
        Q(i)=Q_ed(i)*D2^2*sqrt(g*H(i));
    else
        q(i)=sqrt(1-(sigma*((n(i)/n_R)^2-1)));
        Q(i)=q(i)*Q_R;
        n_ed(i)=n(i)*(D2/sqrt(g*H_R));
        Q_ed(i)=Q(i)/(D2^2*sqrt(g*H_R));
        H(i)=(((n_R*D2)/n_ed(i))^2)/g;
        Q(i)=Q_ed(i)*D2^2*sqrt(g*H(i));
```

```
    end
end

newcm1=2.005*cm2P;
newalpha1=atan(newcm1/cu1)*(180/pi);
newH_R=u1*cu1/g;
newQ_R=newcm1*pi*D1*B1;

for i=1:length(n)
    if (1-(sigma*((n(i)/n_R)^2-1)))<0
        q(i)=-sqrt(abs(1-(sigma*((n(i)/n_R)^2-1))));
        newQ(i)=q(i)*newQ_R;
        n_ed(i)=n(i)*(D2/sqrt(g*H_R));
        Q_ed(i)=newQ(i)/(D2^2*sqrt(g*H_R));
        newH(i)=(((n_R*D2)/n_ed(i))^2)/g;
        newQ(i)=Q_ed(i)*D2^2*sqrt(g*newH(i));
    else
        q(i)=sqrt(1-(sigma*((n(i)/n_R)^2-1)));
        newQ(i)=q(i)*newQ_R;
        n_ed(i)=n(i)*(D2/sqrt(g*H_R));
        Q_ed(i)=newQ(i)/(D2^2*sqrt(g*H_R));
        newH(i)=(((n_R*D2)/n_ed(i))^2)/g;
        newQ(i)=Q_ed(i)*D2^2*sqrt(g*newH(i));
    end
end


%%%%%%%%%%%%%%%%%%%%%%%%%%%%%%%%%%%%%%%%%%%%%%%%%%%%%%%%%%%%%%%%%%%%%%%%%%%%%%%
%Extracting data from logfiles

txtfiles = dir('*.txt');
x=1;
for file = txtfiles'
    NumHeaders = 8;
    NumDataLines = 1000;
    fmt = ['%f %f %f %f %f %f %f'];
    fid = fopen(file.name);
    data = textscan(fid, fmt, NumDataLines, 'HeaderLines', NumHeaders);
    fclose(fid);

    %P_inlet    P_outlet        Flow    Torque    RPM    Head    Efficiency
     for y = 1:7
        datamean(y) = mean(data{y});
        datamatrix(x,y) = datamean(y);
        [f(x,y)] = xErr(data{y}, 0.05);
```

```
112         end
113        x=x+1;
114    end
115
116    P1 = datamatrix(:,1).*1000;
117    P2 = datamatrix(:,2).*1000;
118    Qtest = datamatrix(:,3).*(3600/1000);
119    T = datamatrix(:,4);
120    rpm = datamatrix(:,5);
121    Htest = datamatrix(:,6);
122    eta = datamatrix(:,7);
123
124    %Finding BEP: max efficiency value and location
125    PowT = [0.6 0.51 0.42 0.36 0.27 0.22 0.19 0.15 0.11 0.065 0.025 0.005 -0.02 -0.06 -0.08 -0.1 -0.11 -0.12];
126    for i = 1:length(Qtest)
127        etaT(i) = (PowT(i)*1000)/(rho*g*(Qtest(i)/3600)*Htest(i));
128    end
129    [M,I]=max(etaT);
130    Q_Rtest=datamatrix(I,3)*(3600/1000);
131    H_Rtest=datamatrix(I,6);
132
133    %calibration uncertainties
134    fP1cal = 0.00495;
135    fP2cal = 0.01154;
136    fQcal = 0.00231;
137    fTcal = 0.005633;
138    fZ = 0.00027;
139
140    %test uncertainties
141    f(:,1)=f(:,1)./10;
142    %Total uncertainty
143    fQtot = sqrt(fQcal^2+f(:,3).^2);
144    fP1tot = sqrt(fP1cal^2+f(:,1).^2);
145    fP2tot = sqrt(fP2cal^2+f(:,2).^2);
146    fPtot = sqrt(fP1tot.^2+fP2tot.^2);
147    fetaT =0.05;
148    %mean
149    meanfP1 = mean(f(:,1));
150    meanfP2 = mean(f(:,2));
151    meanfQ = mean(f(:,3));
152    %total mean
153    maxfQtot = sqrt(fQcal^2+meanfQ^2);
154    maxfP1tot = sqrt(fP1cal^2+meanfP1^2);
155    maxfP2tot = sqrt(fP2cal^2+meanfP2^2);
156
```

```
157 %derived uncertainties
158 deltaP = P1-P2;
159 for i=1:length(Qtest)
160     fHder(i) = sqrt((a^2*deltaP(i)^2*fPtot(i)^2 + Qtest(i)^4*rho^2*fQtot(i)^2 + Z^2*rho^2*g^2*a^2*fZ^2)/(deltaP
            (i)^2*a^2 + deltaP(i)*Qtest(i)^2*rho*a + 2*deltaP(i)*Z*rho*g*a^2 + (Qtest(i)^4*rho^2/4) + (Qtest(i)^2*Z
            *rho^2*a*g) + Z^2*rho^2*g^2*a^2));
161 end
162 maxfHder = max(fHder);
163
164 %Empirical correlations
165 Hsharma = H_pump/eta_pump^(1.2);
166 Qsharma = Q_pump/eta_pump^(0.8);
167
168 %Plotting predicted Q_ed-n_ed
169 figure;
170 plot(n_ed,Q_ed)
171 title('Q_{ed} - n_{ed} diagram')
172 ylabel('Q_{ed}')
173 xlabel('n_{ed}')
174 legend('Predicted PAT characteristic','Location','northeast')
175
176 %Plotting predicted H-Q
177 ind2 = H>0 & H<30;
178 figure;
179 plot(Q(ind2).*3600,H(ind2),'--b')
180 hold on
181 plot(Q_R.*3600,H_R,'r*','markers', 10)
182 txt1 = ['\uparrow Symmetry BEP: H_R=' num2str(round(H_R,2)), 'm , Q_R=' num2str(round(Q_R.*3600,2)), 'm^3/h'];
183 txt1 = ['Symmetry BEP: '];
184 txt4 = ['H_R=' num2str(round(H_R,2)), 'm'];
185 txt5 = ['Q_R=' num2str(round(Q_R.*3600,2)), 'm^3/h \rightarrow'];
186 text(3,13,{txt1, txt4,txt5},'FontSize',11)
187
188 %Plotting Sharma
189 plot(Qsharma.*3600,Hsharma,'m*','markers', 10)
190 %txt2 = ['\leftarrow Sharma BEP: H_R=' num2str(round(Hsharma,2)), 'm, Q_R=' num2str(round(Qsharma.*3600,2)), 'm
        ^3/h'];
191 %text(Qsharma.*3600,Hsharma,txt2,'FontSize', 11)
192 %txt2 = ['Sharma BEP: '];
193 %txt4 = ['H_R=' num2str(round(Hsharma,2)), 'm'];
194 %txt5 = ['Q_R=' num2str(round(Qsharma.*3600,2)), 'm^3/h \rightarrow'];
195 %text(6,13,{txt2, txt4,txt5},'FontSize',11)
196
197 %Plotting testdata
198 errorbar(Qtest,Htest,fHder'.*Htest,fHder'.*Htest,fQtot.*Qtest,fQtot.*Qtest,'k');
```

```
plot(Qtest,Htest,'r')
plot(Q_Rtest, H_Rtest,'b*','markers', 10)
txt3 = ['\leftarrow BEP: H=' num2str(round(H_Rtest,2)), 'm , Q=' num2str(round(Q_Rtest,2)), 'm^3/h'];
text(Q_Rtest,H_Rtest,txt3,'FontSize', 11)

%Plotting NEW predicted H-Q
ind2 = H>0 & H<30;
plot(newQ(ind2).*3600,newH(ind2),'b')
plot(newQ_R.*3600,newH_R,'r*','markers', 10)
txt6 = ['\uparrow Symmetry BEP: H_R=' num2str(round(newH_R,2)), 'm , Q_R=' num2str(round(newQ_R.*3600,2)), 'm
    ^3/h'];
%txt1 = ['Symmetry BEP: '];
%txt4 = ['H_R=' num2str(round(H_R,2)), 'm'];
%txt5 = ['Q_R=' num2str(round(Q_R.*3600,2)), 'm^3/h \rightarrow'];
%text(Q_R.*3600,H_R,txt1)
%text(1,14,txt1,'FontSize', 11)
%text(5,13,{txt1, txt4,txt5},'FontSize',11)
text(18,10,{txt6},'FontSize',11)


title('H-Q diagram for n_{R}=1450 rpm')
ylabel('H [m]')
xlabel('Q [m^3/h]')
legend('Predicted characteristic 1st improvement', 'Predicted BEP', 'Sharma BEP','Error in H and Q', 'Test
    characteristic', 'Test BEP', 'Predicted characteristic 2nd improvement','Location','northwest')

%Plotting efficiency
figure;
ind3 = etaT>-0.15 & etaT<0.5 ;
errorbar(Qtest(ind3),etaT(ind3),fetaT.*etaT(ind3),fetaT.*etaT(ind3),fQtot(ind3).*Qtest(ind3),fQtot(ind3).*Qtest
    (ind3),'k');
hold on
plot(Qtest(ind3),etaT(ind3),'b', 'linewidth',1)
grid on
plot(Q_Rtest,M,'r*','markers', 10)
txt2 = ['\uparrow \eta = ' num2str(round(M,3))];
text(17.9,0.36,txt2, 'FontSize', 12)
title('\eta - Q diagram for n_{R}=1450 rpm')
ylabel('\eta','FontSize', 18)
xlabel('Q [m^3/h]')
legend('Error in \eta and Q', 'Pump efficiency curve', 'Location','southeast')
```

D.2 Pump experimental results

```
clear all
close all
clc

rho = 998.5986;
g = 9.82146516;
Aout = pi*(0.032^2)/4;
Ain = pi*(0.05^2)/4;
a = (Aout*Ain)^2/(Ain^2-Aout^2);
Z = 0.37;

txtfiles = dir('*.txt');
x=1;
for file = txtfiles'
    NumHeaders = 8;
    NumDataLines = 1000;
    fmt = ['%f %f %f %f %f %f %f'];
    fid = fopen(file.name);
    data = textscan(fid, fmt, NumDataLines, 'HeaderLines', NumHeaders);
    fclose(fid);

   %P_inlet    P_outlet        Flow    Torque    RPM    Head    Efficiency
     for y = 1:7
        datamean(y) = mean(data{y});
        datamatrix(x,y) = datamean(y);
        [f(x,y)] = xErr(data{y}, 0.05);
     end
    x=x+1;
end


P1 = datamatrix(:,1)*1000;
P2 = datamatrix(:,2)*1000;
Q = datamatrix(:,3);
T = datamatrix(:,4);
rpm = datamatrix(:,5);
H = datamatrix(:,6);
eta = datamatrix(:,7);

%Finding BEP: max efficiency value and location
PowP = [0.35 0.345 0.34 0.335 0.335 0.33 0.33 0.32 0.32 0.32 0.305 0.305 0.30 0.30 0.295 0.285 0.28 0.265 0.26
    0.255 0.2375 0.2375 0.225 0.215];
for i = 1:length(Q)
```

```
43      etaP(i) = (rho*g*(Q(i)/1000)*H(i))/(PowP(i)*1000);
44
45  end
46  [M,I]=max(etaP);
47  Q_R=datamatrix(I,3);
48  H_R=datamatrix(I,6);
49  etaP(10) = (etaP(9)+etaP(11))/2; %%%
50
51  %calibration uncertainties
52  fP1cal = 0.00495;
53  fP2cal = 0.01154;
54  fQcal = 0.00231;
55  fTcal = 0.005633;
56  fZ = 0.00027;
57
58  %Total uncertainty
59  fQtot = sqrt(fQcal^2+f(:,3).^2);
60  fP1tot = sqrt(fP1cal^2+f(:,1).^2);
61  fP2tot = sqrt(fP2cal^2+f(:,2).^2);
62  fPtot = sqrt(fP1tot.^2+fP2tot.^2);
63
64  %mean
65  meanfP1 = mean(f(:,1));
66  meanfP2 = mean(f(:,2));
67  meanfQ = mean(f(:,3));
68  %total mean
69  maxfQtot = sqrt(fQcal^2+meanfQ^2);
70  maxfP1tot = sqrt(fP1cal^2+meanfP1^2);
71  maxfP2tot = sqrt(fP2cal^2+meanfP2^2);
72
73  %derived uncertainties
74  deltaP = P2-P1;
75  for i=1:length(Q)
76
77  fHder(i) = sqrt((a^2*deltaP(i)^2*fPtot(i)^2 + Q(i)^4*rho^2*fQtot(i)^2 + Z^2*rho^2*g^2*a^2*fZ^2)/(deltaP(i)^2*a
        ^2 + deltaP(i)*Q(i)^2*rho*a + 2*deltaP(i)*Z*rho*g*a^2 + (Q(i)^4*rho^2/4) + (Q(i)^2*Z*rho^2*a*g) + Z^2*rho
        ^2*g^2*a^2));
78
79  end
80  maxfHder = max(fHder);
81
82  figure;
83  subplot(2,1,1)
84  hold on
85  grid on
```

```
errorbar(Q*(3600/1000),H,fHder'.*H*(3600/1000),fHder'.*H*(3600/1000),fQtot.*Q*(3600/1000),fQtot.*Q*(3600/1000),
    'k');
plot(Q*(3600/1000),H,'b')
plot(Q_R*(3600/1000), H_R,'r*', 'markers', 10)
txt1 = ['\downarrow BEP: H=' num2str(round(H_R,2)), 'm , Q=' num2str(round(Q_R*(3600/1000),2)), 'm^3/h'];
text(8.86,6.4,txt1, 'FontSize', 11)
title('H-Q diagram for n_{R}=1450 rpm')
ylabel('H [m]')
xlabel('Q [m^3/h]')
legend('Error in H and Q', 'Pump test characteristic', 'Location','southwest')

fetaP=0.05;
subplot(2,1,2)
hold on
errorbar(Q*(3600/1000),etaP,fetaP.*etaP,fetaP.*etaP,fQtot.*Q*(3600/1000),fQtot.*Q*(3600/1000),'k');
plot(Q*(3600/1000),etaP,'b')
grid on
plot(Q_R*(3600/1000),M,'r*','markers', 10)
txt2 = ['\uparrow \eta = ' num2str(round(M,3))];
text(8.86,0.41,txt2, 'FontSize', 12)
title('\eta - Q diagram for n_{R}=1450 rpm')
ylabel('\eta','FontSize', 18)
xlabel('Q [m^3/h]')
legend('Error in \eta and Q', 'Pump efficiency curve', 'Location','southeast')
```

D.3 Test velocity diagrams

```
clear all
close all
clc

%Rated BEP values from tests
Q_RT = 0.0049863;
Q_RP = 0.0024869;
H_RP=5.91;

%Pump input parameters
n_R=1450; %Rated rotational speed
D1P=0.051; %Inlet diameter
D2P=0.153; %Outlet diameter
B1P=0.0304; %Inlet height
beta2P=29; %Blade angle
B2P=0.005; %Outlet height

%%%%%%%%%%%%%%%%%%%%%%%%%%%%%%%%%%%%%%%%%%%%%%
%Parameters needed to plot velocity diagrams

omega_R=(2*pi*n_R)/60;
cm1P = Q_RP/(pi*B1P*D1P);
u1P = omega_R*(D1P/2);
u2P = omega_R*(D2P/2);
cm2P = Q_RP/(pi*B2P*D2P);
cu2P = u2P-(cm2P/tan(beta2P*pi/180));
%cu2P=(9.82*H_RP)/u2P*0.8

D1T = D2P;
D2T = D1P;
B1T = B2P;
B2T = B1P;
beta1T = beta2P;
u1T = omega_R*(D1T/2);
cm1T = Q_RT/(pi*B1T*D1T)
cu1T=u1T-(cm1T/tan(beta1T*pi/180));
u2T = omega_R*(D2T/2);
cm2T = Q_RT/(pi*B2T*D2T)

alpha2P = atan(cm2P/cu2P)*(180/pi)
alpha1T = atan(cm1T/cu1T)*(180/pi)

%%%%%%%%%%%%%%%%%%%%%%%%%%%%%%%%%%%%%%%%%%%%%
```

```
%Points in order to plot velocity diagrams

p1 = [0  0];
p2 = [-cu2P  0];
p3 = [-u2P  0];
p4 = [-cu2P cm2P];
p5 = [cu1T,  0];
p6 = [u1T,  0];
p7 = [cu1T, -cm1T];
p10 = [0  ,  0];
p11 = [-u1P,  0];
p12 = [0, cm1P];
p13 = [u2T,  0];
p14 = [0, -cm2T];

%Pump outlet, turbine inlet
figure();
subplot(2,1,1)
hold on
plot([p1(1) p2(1)], [p1(2) p2(2)], 'b','LineWidth',1)
plot([p1(1) p3(1)], [p1(2) p3(2)],'b','LineWidth',1);
plot([p2(1) p4(1)], [p2(2) p4(2)],'b','LineWidth',1);
plot([p3(1) p4(1)], [p3(2) p4(2)],'b','LineWidth',1);
plot([p1(1) p4(1)], [p1(2) p4(2)],'b','LineWidth',1);
plot([p1(1) p5(1)], [p1(2) p5(2)],'b','LineWidth',1);
plot([p1(1) p6(1)], [p1(2) p6(2)],'b','LineWidth',1);
plot([p5(1) p7(1)], [p5(2) p7(2)],'b','LineWidth',1);
plot([p1(1) p7(1)], [p1(2) p7(2)],'b','LineWidth',1);
plot([p6(1) p7(1)], [p6(2) p7(2)],'b','LineWidth',1);
title('Actual velocity diagrams: Pump outlet and PAT inlet')
ylabel('m/s')
xlabel('m/s')

%Turbine outlet, pump inlet
subplot(2,1,2)
hold on
plot([p10(1) p11(1)], [p10(2) p11(2)],'b','LineWidth',1);
plot([p10(1) p12(1)], [p10(2) p12(2)],'b','LineWidth',1);
plot([p11(1) p12(1)], [p11(2) p12(2)],'b','LineWidth',1);
plot([p10(1) p13(1)], [p10(2) p13(2)],'b','LineWidth',1);
plot([p10(1) p14(1)], [p10(2) p14(2)],'b','LineWidth',1);
plot([p13(1) p14(1)], [p13(2) p14(2)],'b','LineWidth',1);
title('Actual velocity diagrams: Pump inlet, PAT outlet')
ylabel('m/s')
xlabel('m/s')
```

D.4 Error function

```
function [fx] = xErr(x,a)
Sx=var(x);
ts = tinv([a/2 1-a/2], length(x)-1);

fx=ts(2)*(Sx/sqrt(length(x)));

end
```

APPENDIX E

Risk assessment

NTNU	Kartlegging av risikofylt aktivitet	Utarbeidet av	Nummer	Dato	
		HMS-avd.	HMSRV2601	22.03.2011	
HMS		Godkjent av		Erstatter	
		Rektor		01.12.2006	

Enhet: EPT **Dato:** 19/1 - 2018

Linjeleder: Terese Løvås

Deltakere ved kartleggingen (m/ funksjon):
(Ansv. veileder, student, evt. medveiledere, evt. andre m. kompetanse)

Kort beskrivelse av hovedaktivitet/hovedprosess: Masteroppgave student xx. Tittel på oppgaven.

Er oppgaven rent teoretisk? (JA/NEI): *«JA» betyr at veileder innestår for at oppgaven ikke inneholder noen aktiviteter som krever risikovurdering. Dersom «JA»: Beskriv kort aktiviteteten i kartleggingskjemaet under. Risikovurdering trenger ikke å fylles ut.*

Signaturer: *Ansvarlig veileder:* [signature] *Student:* Øyvind Albert, Sondre Skjoldli

ID nr.	Aktivitet/prosess	Ansvarlig	Eksisterende dokumentasjon	Eksisterende sikringstiltak	Lov, forskrift o.l.	Kommentar
1	Oppbygging av testriss	Torbjørn Nielsen				
2	Testing	"				
3	Reise	"				

NTNU / HMS	Risikovurdering	Utarbeidet av	Nummer	Dato	
		HMS-avd.	HMSRV2603	22.03.2011	
		Godkjent av		Erstatter	
		Rektor		01.12.2006	

Enhet: EPT **Dato:** 19/1 -2018

Linjeleder: Terese Løvås

Deltakere ved kartleggingen (m/ funksjon):
(Ansv. Veileder, student, evt. medveiledere, evt. andre m. kompetanse)

Risikovurderingen gjelder hovedaktivitet: Masteroppgave student xx. Tittel på oppgaven.

Signaturer: *Ansvarlig veileder:* [signature] *Student:* Øyvind Albert, Sondre Skjoldli

ID nr	Aktivitet fra kartleggings-skjemaet	Mulig uønsket hendelse/ belastning	Vurdering av sannsyn-lighet	Vurdering av konsekvens:				Risiko-Verdi (menn-eske)	Kommentarer/status Forslag til tiltak
			(1-5)	Menneske (A-E)	Ytre miljø (A-E)	Øk/ materiell (A-E)	Om-dømme (A-E)		
1		Personskade	1	A				A1	
2		Personskade	1	A				A1	
3		Personskade	1	D				D1	

NTNU	Risikovurdering	Utarbeidet av	Nummer	Dato	
		HMS-avd.	HMSRV2603	22.03.2011	
HMS		Godkjent av		Erstatter	
		Rektor		01.12.2006	

Sannsynlighet vurderes etter følgende kriterier:

Svært liten 1	Liten 2	Middels 3	Stor 4	Svært stor 5
1 gang pr 50 år eller sjeldnere	1 gang pr 10 år eller sjeldnere	1 gang pr år eller sjeldnere	1 gang pr måned eller sjeldnere	Skjer ukentlig

Konsekvens vurderes etter følgende kriterier:

Gradering	Menneske	Ytre miljø Vann, jord og luft	Øk/materiell	Omdømme
E Svært Alvorlig	Død	Svært langvarig og ikke reversibel skade	Drifts- eller aktivitetsstans >1 år.	Troverdighet og respekt betydelig og varig svekket
D Alvorlig	Alvorlig personskade. Mulig uførhet.	Langvarig skade. Lang restitusjonstid	Driftsstans > ½ år Aktivitetsstans i opp til 1 år	Troverdighet og respekt betydelig svekket
C Moderat	Alvorlig personskade.	Mindre skade og lang restitusjonstid	Drifts- eller aktivitetsstans < 1 mnd	Troverdighet og respekt svekket
B Liten	Skade som krever medisinsk behandling	Mindre skade og kort restitusjonstid	Drifts- eller aktivitetsstans < 1uke	Negativ påvirkning på troverdighet og respekt
A Svært liten	Skade som krever førstehjelp	Ubetydelig skade og kort restitusjonstid	Drifts- eller aktivitetsstans < 1dag	Liten påvirkning på troverdighet og respekt

Risikoverdi = Sannsynlighet x Konsekvens
Beregn risikoverdi for Menneske. Enheten vurderer selv om de i tillegg vil beregne risikoverdi for Ytre miljø, Økonomi/materiell og Omdømme. I så fall beregnes disse hver for seg.

Til kolonnen "Kommentarer/status, forslag til forebyggende og korrigerende tiltak":
Tiltak kan påvirke både sannsynlighet og konsekvens. Prioriter tiltak som kan forhindre at hendelsen inntreffer, dvs. sannsynlighetsreduserende tiltak foran skjerpet beredskap, dvs. konsekvensreduserende tiltak.

NTNU	Risikomatrise	utarbeidet av	Nummer	Dato	
		HMS-avd.	HMSRV2604	08.03.2010	
		godkjent av		Erstatter	
HMS/KS		Rektor		09.02.2010	

MATRISE FOR RISIKOVURDERINGER ved NTNU

KONSEKVENS						
	Svært alvorlig	E1	E2	E3	E4	E5
	Alvorlig	D1	D2	D3	D4	D5
	Moderat	C1	C2	C3	C4	C5
	Liten	B1	B2	B3	B4	B5
	Svært liten	A1	A2	A3	A4	A5
		Svært liten	Liten	Middels	Stor	Svært stor
		SANNSYNLIGHET				

Prinsipp over akseptkriterium. Forklaring av fargene som er brukt i risikomatrisen.

Farge		Beskrivelse
Rød		Uakseptabel risiko. Tiltak skal gjennomføres for å redusere risikoen.
Gul		Vurderingsområde. Tiltak skal vurderes.
Grønn		Akseptabel risiko. Tiltak kan vurderes ut fra andre hensyn.